Skoltech

Skolkovo Institute of Science and Technology

Doctoral Thesis

by

EVGENIA P. GILSHTEYN

Doctoral Program in Materials Science and Engineering

COMPONENTS FOR STRETCHABLE ELECTRONICS BASED ON SINGLE-WALLED CARBON NANOTUBES

Supervisor
Professor Dr. Sc. Albert G. Nasibulin

Moscow – 2018

Abstract

Wearable and stretchable electronics is urgently developing field of engineering and applied physics, which requires novel forms of conductors as the essential device components. Despite advances in the performance of existing classes of wearable electronic devices and miniaturization of wearable integrated circuits, mechanical design in wearable technology remains conceptually old: brittle components and bulky devices are encapsulated in elastomeric packaging. Conventionally used thin metallic films on elastomeric substrates can accommodate strain (less than 10%) by means of controlled fracture or buckling and they are generally opaque. Conductive polymers can be buckled to form stretchable transparent electrodes, but topographic buckles may be incompatible with devices that require planar interfaces. Thus, new materials are required for transparent, conductive and highly stretchable electrodes.

Electronics based on nanomaterials have been attracting interest recently due to their strain sensing characteristics. However, along with the sensitivity during stretching stable performance of the whole device or system is needed. Here, we report about thin films of single-walled carbon nanotubes (SWCNTs), which can be used as the key component of different electronic devices. The electrical and optical properties of these devices can exhibit excellent characteristics due to a combination of high elastic moduli and outstanding optoelectrical properties of the SWCNTs.

We fabricated various devices and systems, where SWCNTs-based structures play role of passive and active parts of electronic circuit: stretchable electrically conductive hydrogels and poly(dimethylsiloxane) (PDMS) electrodes, strain sensors, highly stretchable and flexible supercapacitors and piezo-supercapacitor systems based on them. Firstly, the stretching mechanism of SWCNT/PDMS structures (i.e., SWCNT thin films deposited on PDMS substrate) were investigated by means of *in situ* scanning electron microscopy (SEM) and compared with the computational studies. Highly transparent, electrically conductive, stretchable structures of tough hydrogels modified by SWCNTs were applied as skin-like passive electrodes and active finger-mounted joint motion sensors. Stretchable all-solid supercapacitors based on SWCNTs have been successfully stretched up to 120% with practically no variation in the electrochemical performance

2

after 1000 stretching cycles and 1000 charging–discharging cycles. High-performance, stable, low equivalent series resistance all-nanotube stretchable supercapacitor based on SWCNTs film electrodes and a boron nitride nanotube separator demonstrates electrochemical double layer capacitance mechanism in a two-electrode test cell configuration and retains 96% of its initial capacitance after more than 20 000 electrochemical charging/discharging cycles and withstands at least 1000 cycles of stretching with low resistance of 250 Ω. Finally, integration of such supercapacitors into a flexible piezo-supercapacitor system with poly(vinylidene-trifluoroethylene) film to harvest and store the energy was also demonstrated. An open circuit voltage of the flexible and transparent supercapacitor reached 500 mV within 20 s during the mechanical action, which allow us to further extend it for providing sustainable power source of various types of sensors integrated into wearable units.

The stretchable, transparent SWCNT based components and devices were prepared without dispersion in an elastic matrix, without time consuming and expensive lithographic techniques and patterned simply using dry transfer method. In the future, it could be possible to use these principles, materials and devices to design electronics that "echo and imitate the natural world by bending, stretching and flexing" and make sense as technology integrated more and more into our lives, our environments, and even our bodies.

List of publications

1. Evgenia Gilshteyn, Albert G. Nasibulin, Aerosol synthesized carbon nanotube films for stretchable electronic applications, Proceedings of the 15th IEEE International Conference on Nanotechnology, 978-1-4673-8156-7, 893-896 (2015).

2. Evgenia P. Gilshteyn, Tanja Kallio, Petri Kanninen, et al., Stretchable and Transparent supercapacitors based on aerosol synthesized carbon nanotube films, RSC Advances, 6, 93915-93921 (2016).

3. Evgenia P. Gilshteyn, Daler Amanbayev, Anton S. Anisimov, Tanja Kallio & Albert G. Nasibulin, All-nanotube stretchable supercapacitor with low equivalent series resistance, Scientific Reports, 7, 17449 (2017).

4. Evgenia P. Gilshteyn, Daler Amanbaev, Maxim V. Silibin, Artem Sysa, Anton S. Anisimov, Tanja Kallio, Albert G. Nasibulin, Flexible self-powered piezo-supercapacitor system for wearable electronics, Nanotechnology, 29, 325501 (2018).

5. Evgenia P. Gilshteyn, Shaoting Lin, Vladislav A. Kondrashov, Daria S. Kopylova, Alexey P. Tsapenko, Anastasios J. Hart, Xuanhe Zhao, Albert Nasibulin, A one-step method of hydrogel modification by single-walled carbon nanotubes for highly stretchable and transparent electronics, ACS Applied Materials & Interfaces, 10, 33, 28069-28075 (2018).

6. Evgenia P. Gilshteyn, Georgy Savostyanov, Stepan Romanov, Daria S. Kopylova, Artem Zyktin, Anton S. Anisimov, Olga E. Glukhova, Albert G. Nasibulin, Strain-induced properties of single-walled carbon nanotube films on PDMS substrates, submitted to ACS Nano (2018).

Other featured publications

1. Laura Martínez-Sartia,Pertegása, María Monrabal-Capilla, **Evgenia P. Gilshteyn**, et al., Flexible light-emitting electrochemical cells with single-walled carbon nanotube anodes, Organic Electronics, 30, 36–39 (2016).

2. Alexandra L. Gorkina, Alexey P. Tsapenko, **Evgenia P. Gilshteyn** et al., Transparent and conductive hybrid graphene/carbon nanotube films, Carbon, 100, 501-507 (2016).

3. Partha P Pal, **Evgenia Gilshteyn**, Hua Jiang, Marina Timmermans, et.al., Single-walled carbon nanotubes coated with ZnO by atomic layer deposition, Nanotechnology, 27, 485709 (2016).

4. Zhukova E. S., Grebenko A. K., Bubis A. V., Prokhorov A. S., Belyanchikov M. A., Tsapenko A. P., **Gilshteyn E. P.,** Kopylova D. S., Gladush Y. G., Anisimov A. S., Anzin V. B., Nasibulin A. G. and Gorshunov B. P., Terahertz-infrared electrodynamics of single-wall carbon nanotube films, Nanotechnology, 28, 445204 (2017).

5. Pramod M Rajanna, **Evgenia P. Gilshteyn**, Timur Yagafarov, Alena K. Aleekseeva, Sergey Anisimov, Alex Neumüller, Oleg Sergeev, Sergey Bereznev, Jelena Maricheva, Albert G. Nasibulin, Enhanced efficiency of hybrid amorphous silicon solar cells based on single-walled carbon nanotubes and polymer composite thin film, Nanotechnology, 29, 105404 (2018).

6. Kopylova D.S., Fedorov F., Alekseeva A., **Gilshteyn E.**, Tsapenko A., Bubis A., Grebenko A., Popov Z., Sorokin P., Anisimov A., Nasibulin A., Holey Single-Walled Carbon Nanotubes for Ultra-Fast Broadband Bolometers, Nanoscale, 2018, Accepted Manuscript.

7. Maria A. Zhilyaeva, Eugene V. Shulga, Ivan V. Sergeichev, **Evgenia P. Gilshteyn**, Anton S. Anisimov, Albert G. Nasibulin, A novel straightforward wet pulling technique to fabricate carbon nanotube fibers, submitted to Advanced Materials.

8. Mehrabimatin B., **Gilshteyn E.**, Buan M. E., Sorsa O., Jiang H., Zad A. I., Shahrokhian S., Kallio T., Nasibulin A., Highly performing NiCo layered double hydroxide and nitrogen-doped graphene based flexible supercapacitor for wearable energy storage, submitted to ACS Appl. Mater. Interfaces.

Acknowledgements

Contents

8

Abbreviations

BNNT – boron nitride nanotube

CGM - coarse-grained modeling

CV – cyclic voltammetry

CVD - chemical vapor deposition

DC – direct current

DMA - differential mobility analyzer

DMF – dimethylformamide

ECG – electrocardiography

ECH - electrically conductive hydrogel

EDLC – electrical double-layer capacitor

EIS – electrochemical impedance spectroscopy

ESR – equivalent series resistance

FET – field-effect transistor

GCD – galvanostatic charge-discharge

IPA – isopropanol

ITO – indium tin oxide

LED – light emitting diode

PDMS - poly(dimethylsiloxane)

PET – polyethylene terephthalate

PVA – polyvinyl alcohol

P(VDF-TrFE) - poly[(vinylidenefluoride-co-trifluoroethylene]

SEM – scanning electron microscopy

SSC - stretchable supercapacitor

SWCNT – single-walled carbon nanotube

TEM – transmission electron microscopy

TS - transparent and stretchable

TSS – transparent stretchable supercapacitor

XRD - X-ray diffraction

List of Figures

11

List of Tables

Chapter 1. Introduction and related work

The development of stretchable and transparent electronics is mostly inspired by the nature and is becoming promising area for next generation of "smart" wearable electronic devices. Among such stretchable electronic devices are those which mimic functions of living species (human [1], animal [2], and even plant [3]) sensing such as artificial skin or muscles [1, 2, 4-8], artificial electronic implants [9, 10], smart prosthetics [11] have been recently developed. Such stretchable and transparent electronics inspired by the nature are promising for huge range of applications in soft robotics, healthcare, human monitoring, human-machine interfaces, and implantable medical systems.

Transparent and stretchable (TS) electronics enable a broad range of new applications such as TS circuits, touch displays and sensors where high transparency and conductivity as well as fully independent operation at large mechanical strain are simultaneously required. Such technological features will allow conformal placement of devices and components on the human skin or any other curved and complicated surface, as well as improve secure operation in consumer electronics applications. Polymers represent the most promising platforms for integration of TS conductors due to their inherent low mechanical stiffness. By present time, numerous soft, flexible and stretchable devices build on polymeric substrates have emerged as platforms capable of digitizing biological signals for healthcare monitoring, which is called "lab-on-skin" [12]. The underlying concept is that these "lab-on-skin" devices can noninvasively measure most of the biometrics required for health monitoring and disease diagnosis. Figure 1 [13] shows examples of soft electronic interfaces located at different places on the human body and developed for both monitoring and measuring such physiological parameters, as temperature, hydration, blood pressure, blood oxygen level, skin mechanics, wound-healing, electrophysiology, and various biomarkers in sweat.
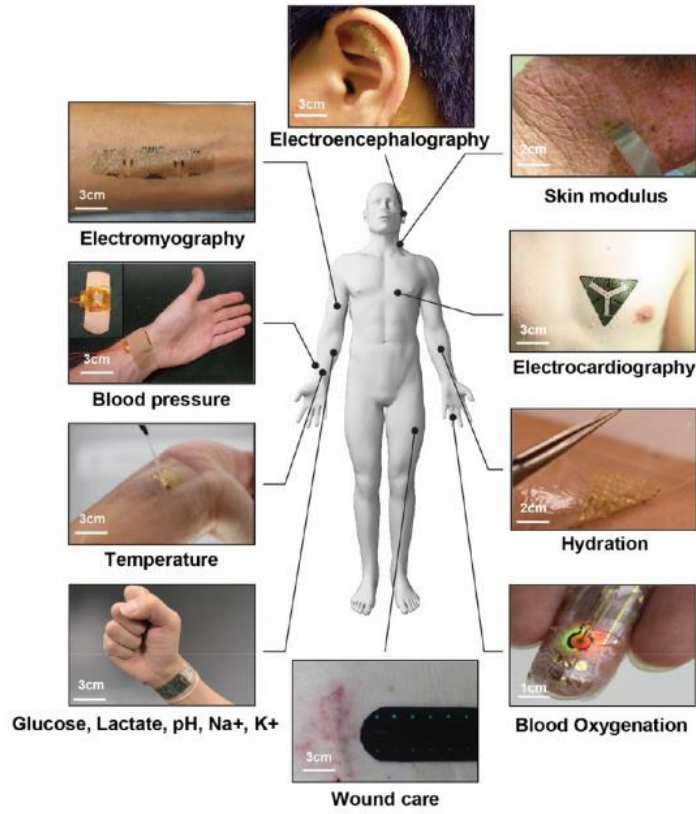
Figure 1. A "lab-on-skin": stretchable/flexible devices for measuring body parameters [12].

However, the methods of new materials for novel electronics development and processing exhibits several challenges. The fabrication of such TS devices could be implemented by two different approaches: (i) geometric engineering of the materials on TS substrates to fabricate TS electronic devices [14-16], and (ii) directly depositing intrinsically transparent and stretchable materials on TS substrates to generate TS electronic devices [17]. The first approach allows to fabricate high performance, stretchability, and stability under mechanical deformation of the TS devices. However, there are several disadvantages such as a complicated fabrication processes, stretching in specific directions only, low device density, low production yield, high cost, and difficulty in manufacturing in general. Some of these disadvantages can be solved by the integration of the intrinsically TS materials, which is possible in frames of second approach. However, the electrical response of the devices in frames of second approach is unstable under

mechanical strain applied. Moreover, it is hard to manufacture intrinsically TS materials (conductors, insulators, and semiconductor materials). Therefore, it is still big unsolved issue of TS electronic devices creation, which would be characterized by high performance, high stretchability, stability, and a simple fabrication process. At the meantime, the TS components include TS conductors, semiconductors, and insulators (Figure 2).
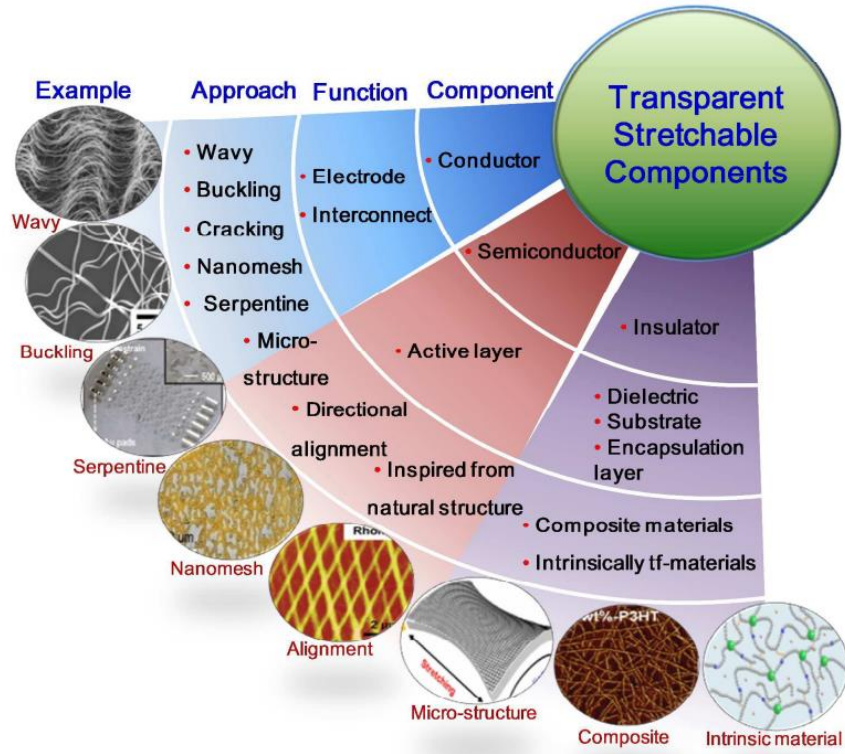
Figure 2. Several approaches to achieve TS components [17].

Transparent conductors are key building blocks for the development of TS electrodes and interconnects, which are the basis of various "lab-on-skin" and other stretchable devices. Films of carbon nanomaterials, such as SWCNTs, have attracted numerous research interests in this area because (1) the long mean-free path of charge carriers in defect-free films results in high conductivity, without the significant decrease of the transparency, and (2) networks of carbon nanomaterials permit elasticity without destroying the structure of the film. SWCNTs are a unique family of carbon-based materials exhibiting exceptional thermal, electronic and mechanical properties, such as excellent electrochemical stability, well-defined one-dimensional structure, low mass

15

density, high mechanical strength and high specific area. As it was already mentioned, SWCNTs can be easily deposited from filter onto practically any substrate and in this case such preparation method is very simple and can be done in a second time scale. For testing flexibility, the CNT films were deposited on a PET substrate, which was bent around 30 000 times with the curvature radius of 1 mm and demonstrated very high stability of SWCNT films. Due to the properties mentioned above, SWCNTs serve as good alternatives for developing new era of stretchable electrodes and sensors.

Chapter 2. Materials and Methods

2.1 Aerosol SWCNT synthesis and film deposition

All carbon nanotubes (CNTs) synthesis methods can be divided into two major groups: physical and chemical techniques based on the carbon atomization. Physical methods can be characterized by high energy input to the carbon source, such as arc-discharge, laser or induction heating evaporation. Chemical methods are based on the CNTs growth due to the decomposition of carbon containing precursors. The obvious advantage of this method, which can be implemented in a lab-scale, is the production of the CNTs at relatively low temperatures. The chemical methods can be further divided into substrate chemical vapor deposition (CVD) and aerosol (floating catalyst) CVD syntheses. After the synthesis and collection on a nitrocellulose filter, CNTs can be easily deposited onto practically any target substrate, so that time-consuming steps of CNT purification from the catalyst, dispersion and deposition processes are avoided. Additionally, aerosol method allows to on-line control of the CNT quality and separate CNTs. As aerosol CVD process could be continuous it becomes one of the most promising methods for the high-yield synthesis of the high quality CNTs at controlled conditions [18 - 21]. One of the most common ways of SWCNT production by aerosol methods is based on thermal decomposition of ferrocene dissolved in different carbon sources. The key to the successful synthesis is the product of CO disproportionation (Boudouard reaction) reaction on the surface of iron particles (1):

$$2CO \leftrightarrow CO_2 + C_{(s)}. \qquad (1)$$
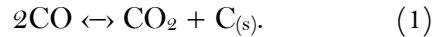
As a result, SWCNTs are collected either by filtering the flow onto a membrane filter, or by an electrostatic collector/precipitator or thermophoretic precipitators. One of the advantages of this method is the possibility to on-line control the quality of CNTs using differential mobility analyzer (DMA). DMA sorts flow products according to their mobility (which depends on the charge and particle size) and condensation particle counter counts the number of particles with the selected nobilities. As a result real-time number-

size distribution of products can be monitored. Thus, SWCNTs collected downstream the reactor form random network on the filter. SEM and TEM images of SWCNT films produced by aerosol method is represented in Figure 3.

(a) **(b)**
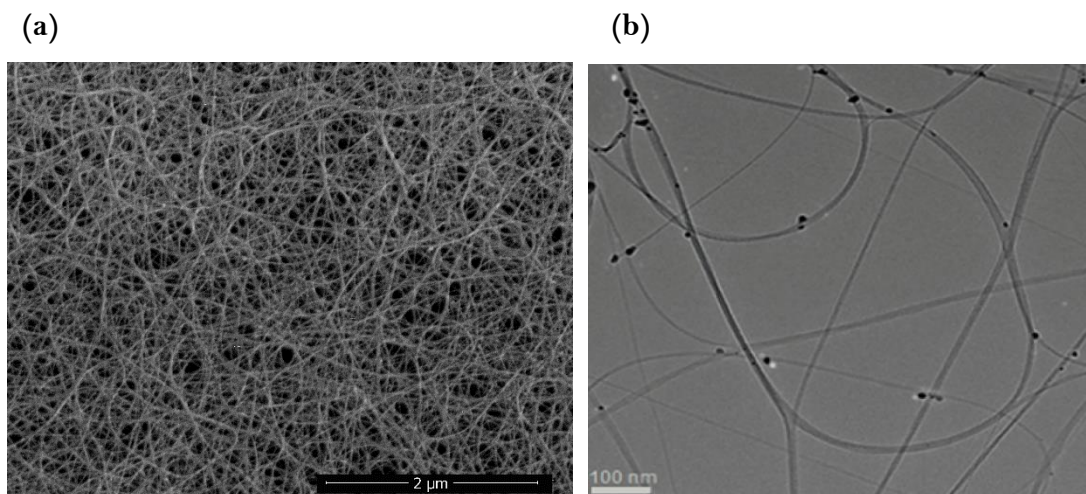
Figure 3. (a) SEM and (b) TEM images of aerosol synthesized SWCNT film.

SWCNT films used in this study have a thickness of approximately 40 nm (with an optical transmittance of 80% at 550 nm). After collection on filter SWCNTs can be easily deposited onto particularly any substrate (glass slide, PET, PDMS, tough hydrogel, silicon wafer, etc.) as it is shown in Figure 4 as an example on tough hydrogel (steps 1 to 5): 1 – cutting of the hydrogel and filter with SWCNTs of the desired shape, 2 – pressing of the SWCNTs to the hydrogel surface, 3 – checking the transferring process and picking up the filter from one of the edges, 4 – peeling off the filter from the hydrogel, 5 – SWCNT film on hydrogel ready to be used for various applications.
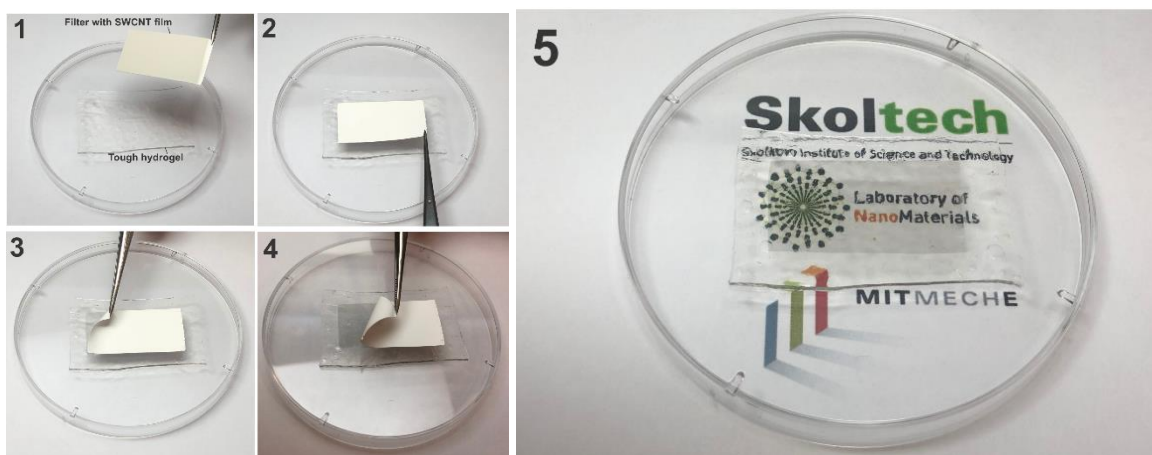
Figure 4. Dry process of SWCNTs film deposition/transfer on tough hydrogel.

2.2 Fabrication of stretchable elastomers

2.2.1 PDMS substrates

PDMS substrates with the thickness of about 0.5 mm were prepared by pouring the mixture of "base" and "curing" agents at a ratio of 10:1 (Sylgard 184, Dow Corning) into circle glass mold, followed by thermal curing at 90°C for 15 minutes. After solidification the PDMS film was cut into required size pieces and peeled off from the glass.

2.2.2 Tough hydrogels

Tough hydrogels utilized in this work were synthesized according to following previously reported protocol. A precursor solution was prepared by mixing 4.1 mL of 4.8 wt% alginate (Sigma, A2033) and 5.5 mL of 18.7 wt% acrylamide (Sigma, A8887). We added 0.2 g N,N-methylenebisacrylamide (Sigma, 146072) as the crosslinker for polyacrylamide and 102 μL of 0.2 M ammonium persulfate (Sigma, 248 614) as an initiator for polyacrylamide. After degassing the precursor solution in a vacuum chamber, we added 200 μL of 1 M calcium sulfate (Sigma, C3771) as the ionic crosslinker for alginate and 8.2

μL N, N, N′, N′-tetramethylethylenediamine (Sigma, T7024–50M) as the crosslinking accelerator for acrylamide. Thereafter, the precursor solution was poured into an acrylic mold and was subjected to ultraviolet light for 60 min with 8 W power and 254 nm wavelength to cure the hydrogel.

2.2.3 PVA-gel electrolyte

A gel containing polyvinyl alcohol (PVA) powder (5 g) and H_2SO_4 (5 g, 95% concentration) in water (50 mL) was used as the electrolyte. It is worth nothing that the strength of the H_2SO_4 was 95%. Then, the viscous solutions were cast onto the SWCNT electrodes, subsequently the two electrodes coated with the gel electrolyte were dried in the air at room temperature for 10 h. While the solution was still viscous, one of the electrolyte coated electrodes was firmly pressed on the other electrolyte coated electrode and the whole assembly was treated at 40°C for 5 h, while the whole supercapacitor became solidified but still fully stretchable.

2.3 Electrical and optical measurements

After deposition of the SWCNTs on different substrates (such as PDMS and hydrogel) SWCNTs/elastic structures were simultaneously tested (by a homemade stretching device) (Figure 5) with two-wire resistance measurements (Digital Multimeter Keysight 34410A). Both edges of the substrates with the deposited SWCNT film were fixed under the clips of a stretching device. For the characterization of optical properties absorbance of the samples was measured by Lambda 1050 UV-vis-NIR spectrophotometer at the wavelength range of 260-2600 nm. The scattering spectra (diffusive part of full transmittance) of substrates at different stretched states were measured using a spectral response measurement system Bentham PVE300. The system is equipped with DTR6 integrating sphere (Ba_2SO_4-coated, 150 mm in a diameter) with approximately 2.5×2.5 mm^2 monochromatic probe beam on the working plane of a sample.
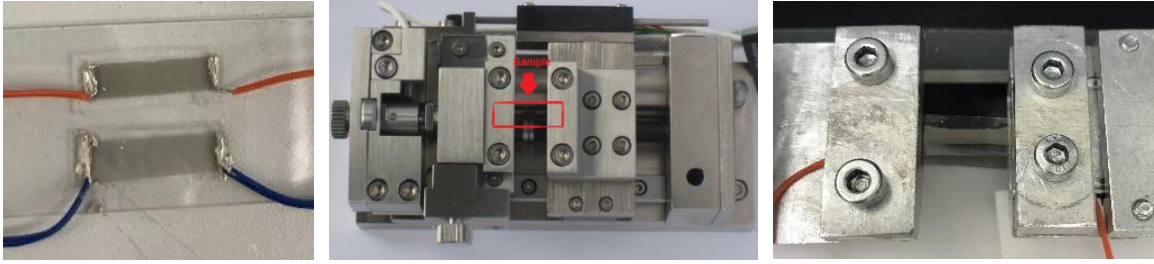
Figure 5. Photographs of the (from left to right): SWCNT/PDMS test samples with silver paste contacts, SEM stage Gatan 200N and homemade stretching device with the structures fixed under the clips.

2.4 TEM and SEM techniques

Morphology of the SWCNT/elastic structures were investigated using FEI Versa Dual Beam scanning electron microscope (environmental mode) with a special tensile stage Gatan 200N (Figure 5) for an *in situ* visualization of stretching/releasing processes. TEM images were obtained with a Tecnai G2 F20 transmission electron microscope with a point resolution of 0.24 nm at 80 kV.

2.5 SWCNT/hydrogel structures integration

In order to fabricate patterned SWCNT films on a hydrogel surface the following technique was used. A template of the SWCNT film pattern was created by graphical software and processed by the CO_2 laser cutting machine (GCC LaserPro Spirit GLS) and computer printing tool. The SWCNT film was patterned according to the created image of the desired circuit by simple burning of the SWCNTs at undesired places. Further hydrogel substrate was pressed against the patterned SWCNT films, and after the deposition, a nitrocellulose filter was peeled off from the surface. A small amount of conductive silver paste was used in order to make contact between the SWCNT film and rigid case of LED. For ECG signal measurements the AD8232 integrated signal conditioning block was used. Three-electrode configuration was realized for signal processing, where firstly commercially available ECG electrodes were connected to right, left hand and right foot. After that SWCNT/hydrogel-based electrodes were attached to the same places.

2.6 Electrochemical characterization of the supercapacitors

The electrochemical measurements and stability of TSSs was studied with an Autolab PGSTAT100 potentiostat (Metrohm) at various scanning regimes. Cyclic voltammograms at different ranges and scan speeds were recorded with an Elins Potentiostat-galvanostat P-40X.

2.7 Coarse-grained molecular dynamics for theoretical modeling

This part of work was carried out by the colleagues from the Department of Physics, Saratov State University – Professor Olga E. Glukhova and Georgy Savostyanov. As full-atom molecular dynamics simulations cannot access the carbon nanotube networks with current computing resources, we use the most suitable model for the theoretical study of the mechanical characteristics of the SWCNT films - so-called coarse (coarse-grained) model. Unlike the atomistic model, when using coarse-grained modeling a group of atoms is combined into one virtual particle. This simplification allows us to consider systems that can simulate processes occurring in films consisting of several thousand of SWCNTs and to investigate in detail the changes in the film structure under inelastic stretching. The model of the SWCNT film was constructed by filling of a 3D box 200 nm long (X axis), 60 nm wide (Y axis), and 50 nm thick (Z axis) with straight SWCNTs. In this case, periodic boundary conditions were applied to the X and Y axes, while the film was confined along the Z axis by two flat van der Waals barriers. The length of the tubes was taken as 50 nm. The choice of this length made it possible to exclude the self-action of nanotubes due to the presence of periodic boundary conditions along the X and Y directions. The uniform filling by SWCNTs was carried out using the Monte Carlo method until the desired density was achieved.

Chapter 3. Results and discussion

3.1 Strain-induced properties of SWCNT films on PDMS substrates

3.1.1 Two approaches of SWCNT films transfer from a filter onto PDMS

For our studies we utilize films of SWCNTs, synthesized by the aerosol CVD method, with a thickness of approximately 40 nm (with an optical transmittance of 80% at 550 nm). However, our method allows to prepare SWCNTs with adjustable transparency from 0 to 99%. After the nitrocellulose filter with SWCNT film is cut in a desired shape (standard size of the samples is 2.0 x 0.5 cm2), it is simply pressed against the PDMS. As SWCNTs have low adhesion to a nitrocellulose filter, the filter is easily peeled off, leaving the SWCNT film on the surface of PDMS. It is worth mentioning that the absence in the need to utilize any liquid for the film preparation makes our approach unique to fabricate highly stretchable conductive structures.

For the first time we show that the same SWCNT films applying two different approaches might possess different behavior depending on the deposition process of the SWCNTs on a PDMS substrate: i) strain-sensitive behavior, where the resistance change can be detected while a certain strain is applied; ii) stable performance, which is independent on the applied strain (Figure 6). The first approach is based on a simple transfer of the SWCNTs from a filter onto the as-prepared PDMS surface, while the second one is based on pre-stretching of the PDMS before the SWCNT film deposition and further strain release (Figure 6).

(a) **Different behavior during stretching**

Strain-sensitive performance

Stable performance
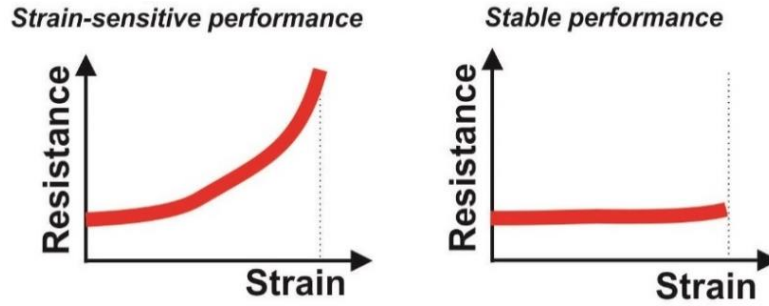
(b)
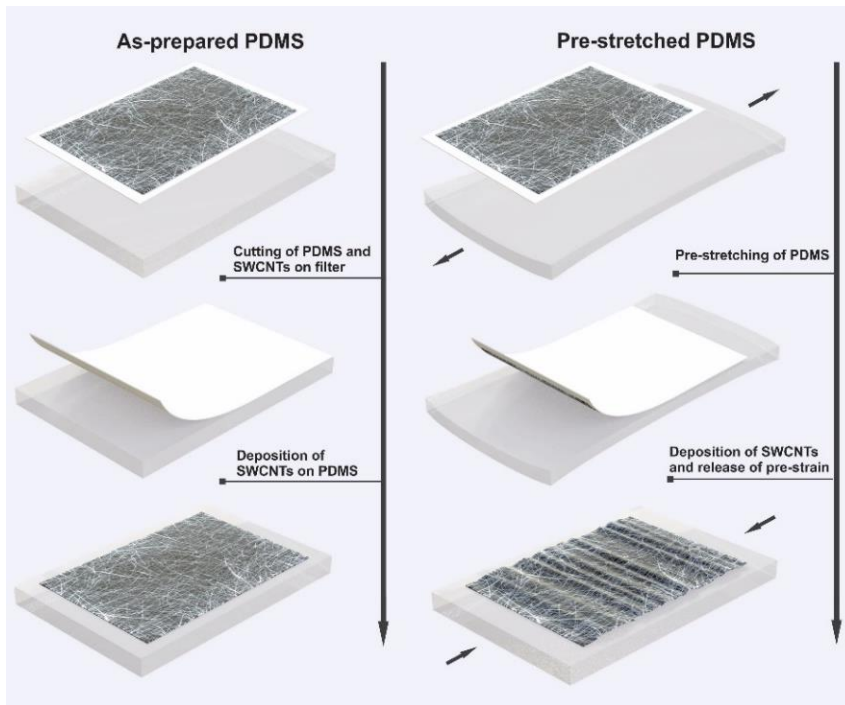
Figure 6. Generic illustration of a) two operational modes of SWCNTs during stretching; b) SWCNT film deposition process realized by two dry transfer approaches: on the as-prepared PDMS and on the pre-stretched PDMS.

3.1.2 Investigation of the SWCNT films morphological changes while stretching

After the SWCNT film deposition on the as-prepared PDMS by the first approach the mechanisms of stretching are in situ studied by means of a special tensile stage loaded into the SEM. The SEM images in Figures 7a-c show the microscale morphology evolution of the SWCNT films from random orientation (Figure 7a) to a densely aligned

microstructure (Figure 7c) in the direction of the strain (the stretching direction is shown in Figure 7d). In order to qualitatively estimate the alignment degree of the SWCNTs we preliminary use Fast Fourier Transform (FFT) algorithm (inset images of Figures 7a-c). For the quantitative analysis of the SWCNT orientation in the films we arrange the image processing of the SEM images, which is based on calculation of local gradients of intensity. As we can see in Fig. 7e the SWCNTs start to be aligned, when a 10% strain is applied. The amount of SWCNTs in the horizontal direction reduces while higher strains applied (peak at 0°). At the same time, the amount of SWCNTs oriented in the direction of the strain applied (peaks at -90 and 90°) increases with further stretching. For this peak points at 10, 50 and 100% strains, the normalized intensities of the SWCNTs distribution are 120, 150 and 190%, respectively. We further investigate behavior of the SWCNT/PDMS structures after the strain release (Figure 7f). This leads to the formation of wrinkles in the direction perpendicular to the strain. Figure 7g is a cross-sectional image of the SWCNTs/PDMS structures after formation of stable wrinkles. It can be easily seen that the SWCNT film repeats wavy form of the PDMS substrate, which proves excellent adhesion of the SWCNT film. Here, in order to perform proper cross-sectioning we deposited a thin layer of gold on top of SWCNTs/PDMS structure. From this image we can also define the mean height of the wrinkles (300 nm) and the mean periodicity (about 0.8 μm).

The same characterization of the morphological changes is conducted for the second approach on PDMS pre-stretched to 30% (Figures 8a-d). From the SEM images we can see that a SWCNT network becomes flat when the strain, higher than the pre-strain value, is applied. The release of the strain leads to the formation of initially wrinkled morphology with the mean wrinkle period of less than 1.0 μm.
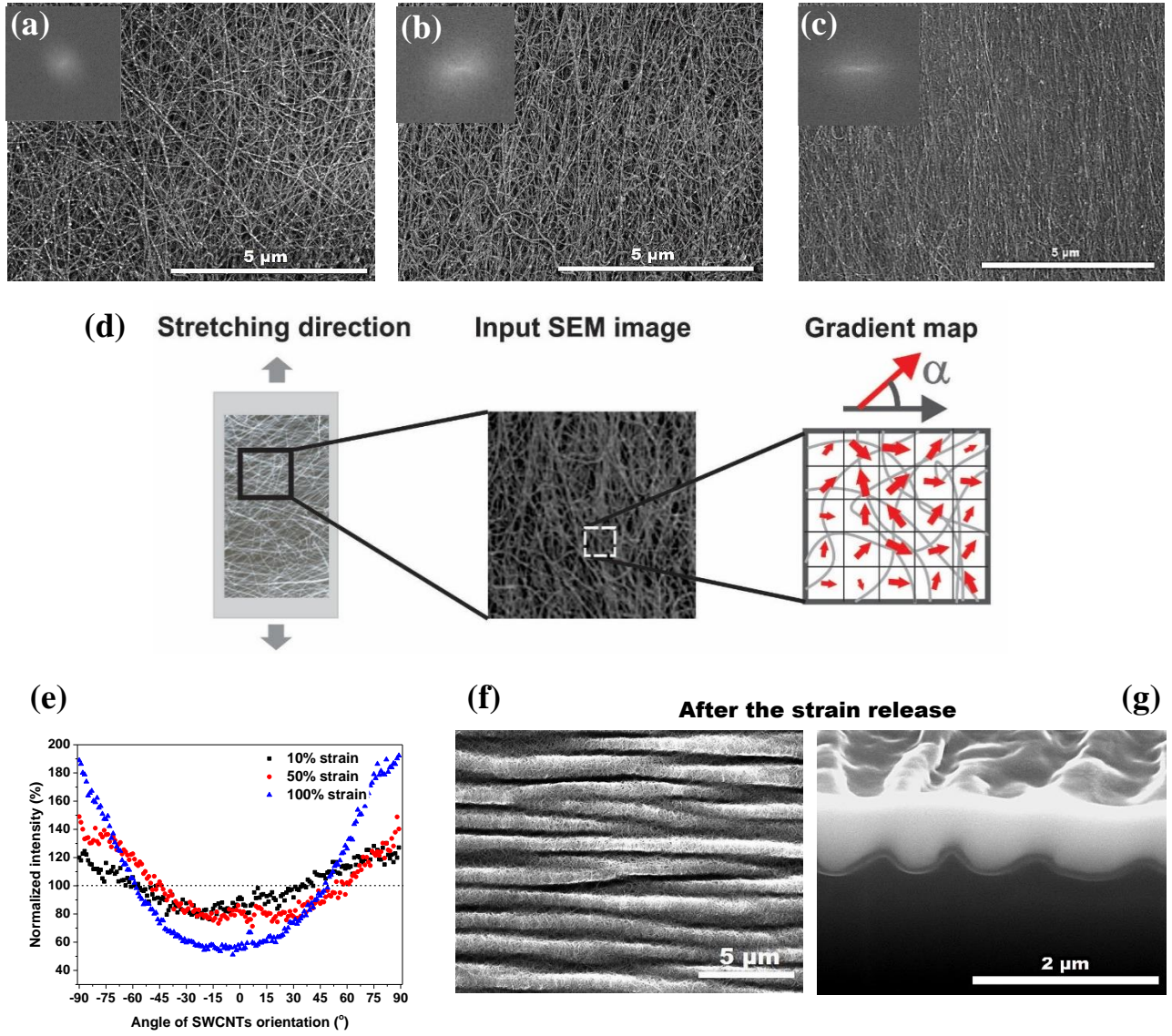
Figure 7. Characterization of SWCNT/PDMS structures prepared by film deposition onto the as-prepared PDMS. SEM images of the structures at a) 10%, b) 50%, c) 100% strains applied. Insets are Fast Fourier Transform (FFT) of the SEM images. d) Scheme of the proposed method for the SWCNT orientation analysis showing e) Changes in the SWCNTs orientations calculated for the local gradients of intensity from SEM images of the structures stretched to 10, 50, 100% strains, normalized to the pristine state. SEM images after the strain release: f) top and g) cross-sectional view.
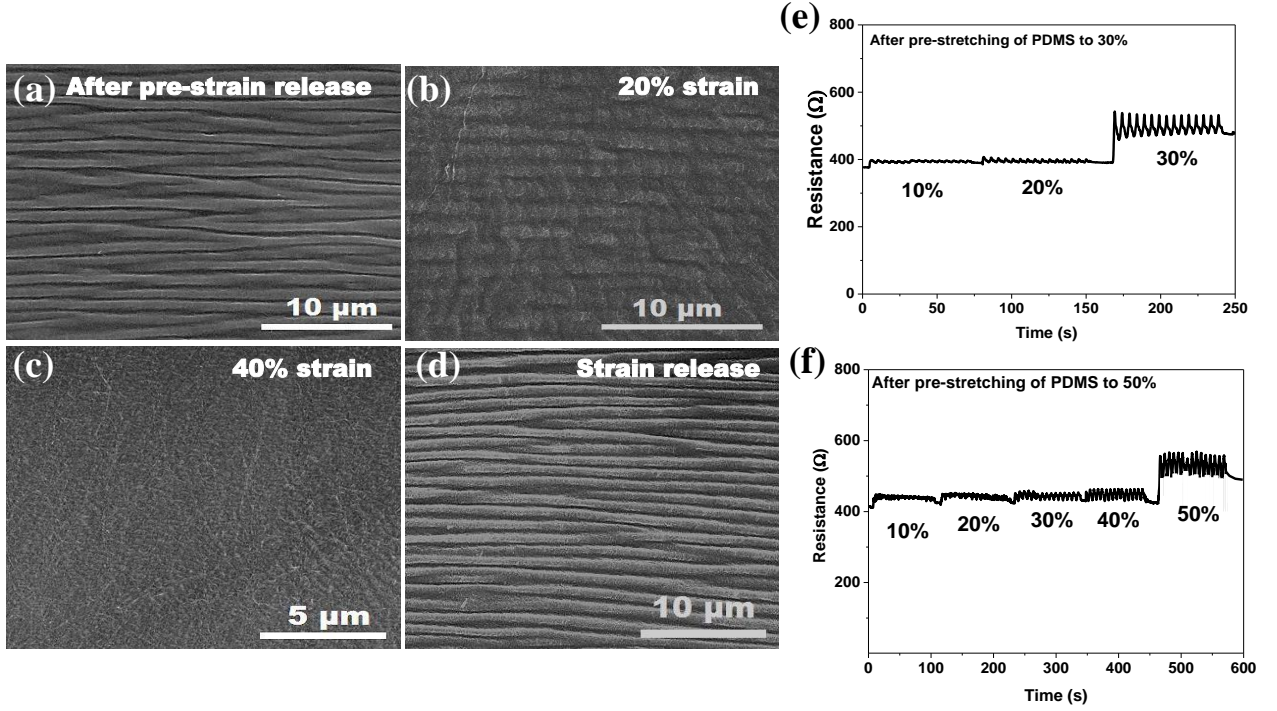
Figure 8. SEM images of the films prepared according to the pre-stretching approach: a) SWCNT film, deposited on a PDMS substrate pre-stretched to 30%, b) the samples stretched to 20% from the released state, c) the samples stretched to 40%, d) the samples after the strain release. Electrical properties of SWCNT films deposited on pre-stretched PDMS. Resistance change of SWCNT film: e) during stretching to a 30% pre-strain value and f) to a 50% pre-strain value.

3.1.3 Electrical properties of the SWCNT/PDMS structures and its computational modeling

Electrical parameters dependence of both film types on stretching with multiple stretching/relaxation cycles under different strain values were further investigated. Electrical properties of SWCNT/PDMS structures fabricated on the as-prepared PDMS during multiple stretching/relaxation cycles under different strains were further investigated. Figure 8a demonstrates the resistance change of the structure while stretched for the first time from 0 to 100% strains with the interval of 10% and 15 cycles at each strain value. As a result, the as-fabricated approach allows us to obtain SWCNT/PDMS structures sensitive to different strains. We measure the sheet resistance of the SWCNT films deposited onto the PDMS substrate by this approach, which becomes about 3 times higher after stretching to 50% compared to the relaxed state (from 100 $\Omega/\square$

27

at 0% strain to 320 $\Omega/\square$ at 50% strain). However, based on this approach we always change the reference 'zero strain state' of the film while applying higher strains. Therefore, we examined the technique of the electrical performance improvement, which is based on several preliminary stretching cycles of the SWCNT/PDMS structure, to the maximum 100% strain before the first stretching (Figure 8b). By this method we were able to remove the floating baseline up to 90% strain and achieve the stable 'zero strain state' of the resistance during each releasing cycle, which could be useful for the accurate sensing capabilities. The relative change in the resistance $\Delta R/R0$ for the as-prepared PDMS approach varies from 0.4 to 20.1 for strains from 10 to 100%, while for the same approach with zero level stabilization the corresponding values are: from 0.03 to 2.1.

A comparative study of the electrical properties of the SWCNT films is conducted for the first stretching cycle of the SWCNT/PDMS structures from 0 to 100% strain using the coarse-grained modelling (CGM). After the uniform filling of the cell by the SWCNTs using the Monte Carlo method (Figure 9c), minimization of the total energy and bundling of the SWCNTs, calculation of the resistance is performed along with the SWCNT film stretching. The value of contact resistance between SWCNTs is used as the fitting parameter of the model and is varied from 1 to 100 kΩ. Figure 9d shows good correlation and qualitative agreement of the dependence obtained using the contact resistance between tubes of 13 kΩ with the experimental curve obtained for SWCNT/PDMS sample.

The pre-stretching approach is demonstrated to be promising for realization of structures with stable properties while being stretched (Figure 8e). Here, we were able to achieve the stable resistance of 400 Ω for 10% and 20% strains with the increase in the resistance starting from 30% pre-strain. The relative change in the resistance is 0.05, 0.07 and 0.4 for 10, 20 and 30% strain, respectively. This behavior is confirmed for structures obtained on PDMS pre-stretched to 50% strain (Figure 8f). Noisy background of the line here is the artefact of contact pads deformation while stretching. The values of the relative resistance change are quite low: 0.06, 0.08, 0.1, 0.12 and 0.36 for stains 10, 20, 30, 40 and 50%, respectively.
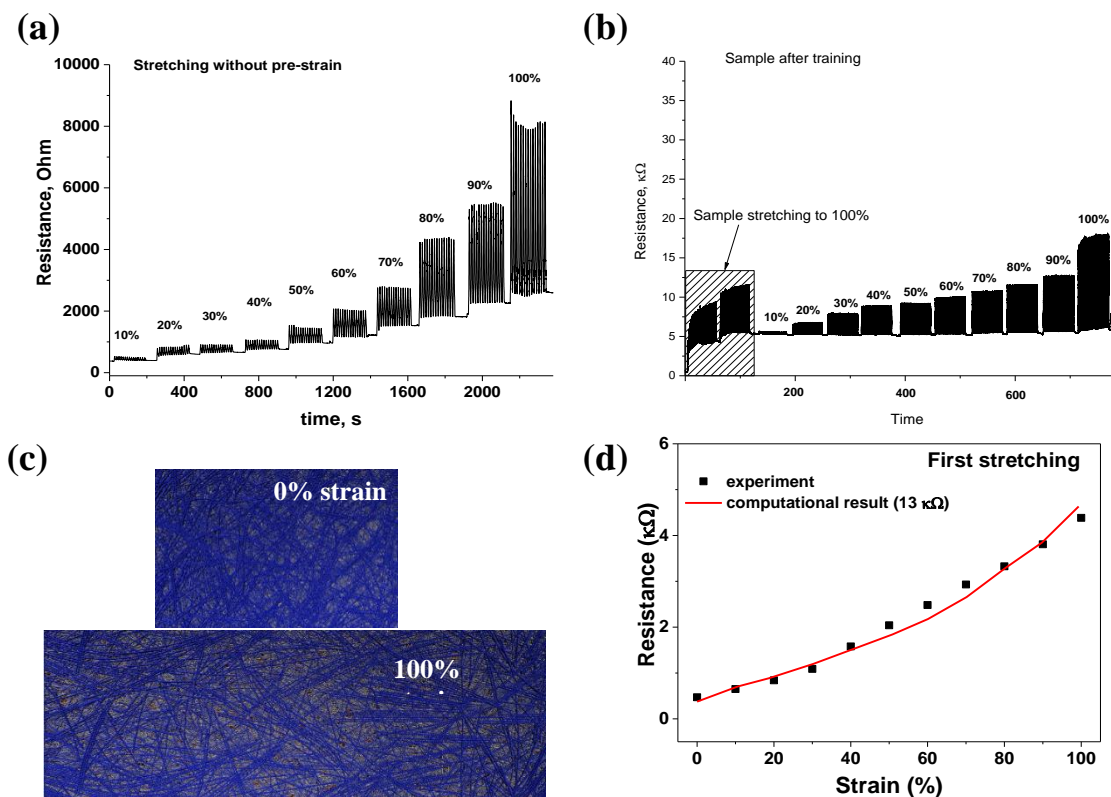
Figure 9. Resistance change of SWCNT film: a) on as-fabricated PDMS (15 cycles of stretching to a certain strain value from 0% to 100%); b) on PDMS trained to 100% before stretching. Coarse-grained model (CGM) of SWCNTs stretching: c) Simulated morphology of the SWCNTs before stretching and at 100% strain applied, d) Theoretically predicted resistance change of SWCNT film on PDMS stretched from 0 to 100% strain compared to the experimental results.

3.1.4 Application of the proposed approach to the commercially available SWCNTs

We applied the proposed stretching approaches to commercial SWCNTs, such as TUBALL™ (OCSiAl Ltd.), as a water dispersion. Step by step process of the commercial TUBALL SWCNT film deposition on the as-prepared PDMS substrate is described in the Experimental section. Application of the as-prepared stretching approach described in Figure 1b leads to appearance of microcracks in the film at 10% strain with the increase of crack density during stretching to higher strains (Figure 10a–c). After the strain release increased density and intensity of wrinkles of the structure is observed (Figure 10d). As

the SWCNTs are obtained from water dispersion after the filtration and drying the films get densified which affects the stretchability and mechanical toughness of the film. For a comparison the aerosol synthesized SWCNTs used in this study being transferred onto the PDMS substrate without any liquid treatment behave as an 'alive' network, where SWCNTs occupy the most energetically favorable positions under the strain without the breakage of the network, therefore making this method the most suitable for highly stretchable applications. Thus, our simple and straightforward process of SWCNT/PDMS structures fabrication provides an easy and feasible method for a scaled-up process for potential stretchable electronic materials and devices creation, making aerosol-synthesized SWCNT films a good alternative for developing new era of stretchable electrodes and sensors.
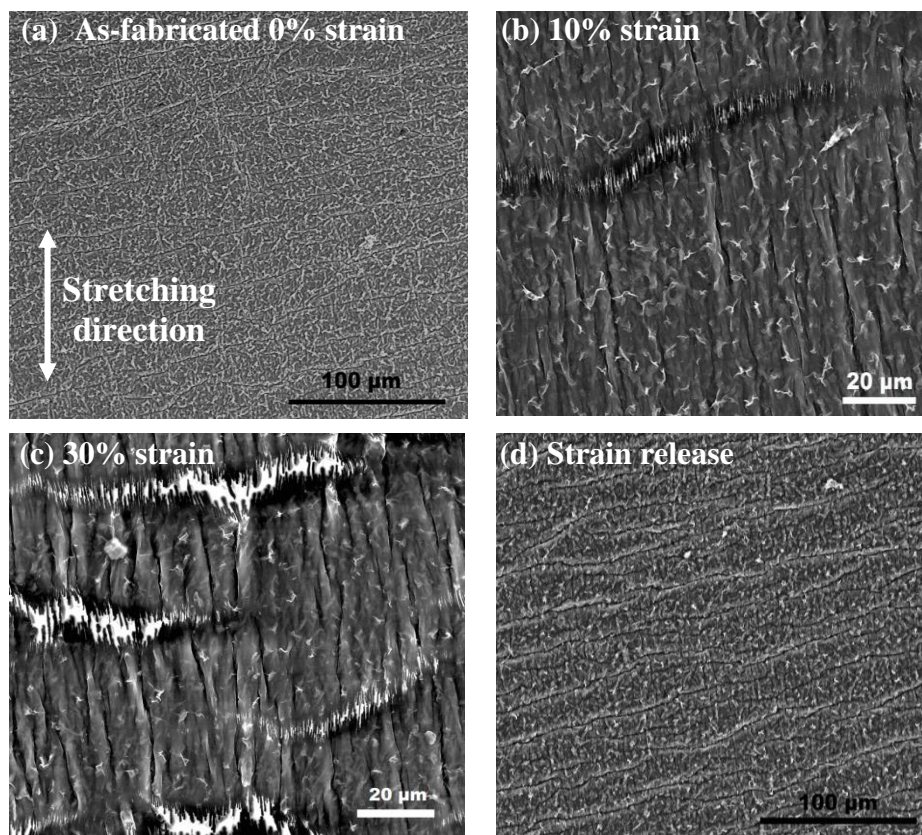
Figure 10. SEM images of the SWCNT films fabricated from water dispersion on the as-prepared PDMS substrate: a) initially without any strain applied; b) 10% strain applied leading to the appearance of micro cracks, c) 30% strain increasing the density of the cracks; d) overview of the film morphology after the strain release.

30

3.2 A one-step method of hydrogel modification by SWCNTs

Hydrogels are soft materials, which have enabled diverse modern technologies, including tissue engineering [22-24], drug delivery [25], biomedical devices [26], microfluidics [27, 28], stretchable and bio-integrated electronics [29] and soft robotics [30, 31]. Furthermore, hydrogels with similar physiological and mechanical properties to a human skin represent an ideal material for electronics and devices to achieve long-term effective bio-integrations [32, 33]. However, commonly used electrically conductive hydrogels (ECHs) [34, 35] are usually produced in the form of composites, which consists of hydrogels and conductive fillers such as silver nanowires [36], PEDOT:PSS [37], graphene [38], *etc.* However, an effective incorporation and dispersion of SWCNTs in the matrices of polymeric hydrogels remain a great challenge due to their agglomeration and presence of surfactants. Moreover, such materials do not possess desired mechanical robustness, which limits the stretchability of ECHs.

The technique proposed in this study allows us to utilize high water content and transparency with good electrical and mechanical properties without loses in both SWCNTs and hydrogel functionalities. Using this approach, we realize mechanically robust, highly stretchable, biocompatible, conductive and transparent SWCNT/hydrogel structures and demonstrate their applications as finger-mounted joint motion sensors and electrocardiographic electrodes. The advantages of the proposed structures in terms of conductivity, stretchability, transparency and applicability for electronic circuit creation are highlighted in Table 1.

Table 1. Comparison between main properties of electrically conductive hydrogels with different fillers and SWCNT/hydrogel structures, proposed in this study.

Materials / Properties	Electrical wire [26]	Graphene [95]	Silver nanowires [37]	PEDOT:PSS [38]	SWCNTs (this study)
Conductivity	50 Ω	From 100 Ω	From 479 Ω	More than 1MΩ	From 120 Ω
Stretchability	Up to 200%	No, only bending	No, only bending	No	Up to 100%
Transparency	No	No	Small, highly reflective	No	High, up to 70%

Scalability for electronic circuits	No due to complicated serpentine form	No due to 3D composite structure	Yes, by AgNWs micro patterning	No due to 3D composite structure	Yes, by patterning with laser cutter

3.2.1 SWCNT film deposition process on a hydrogel surface

The process of the SWCNT films deposition on a hydrogel surface is similar to one, which was demonstrated previously for the PDMS-based structures (Chapter 3.1) and can be implemented in two similar ways. The photographs of the stretched tough hydrogel and obtained SWCNT/hydrogel structure are presented in Figure 11. This demonstrates high transparency of the SWCNT/hydrogel structures, which retain even in the stretched state.

(a)   **(b)**
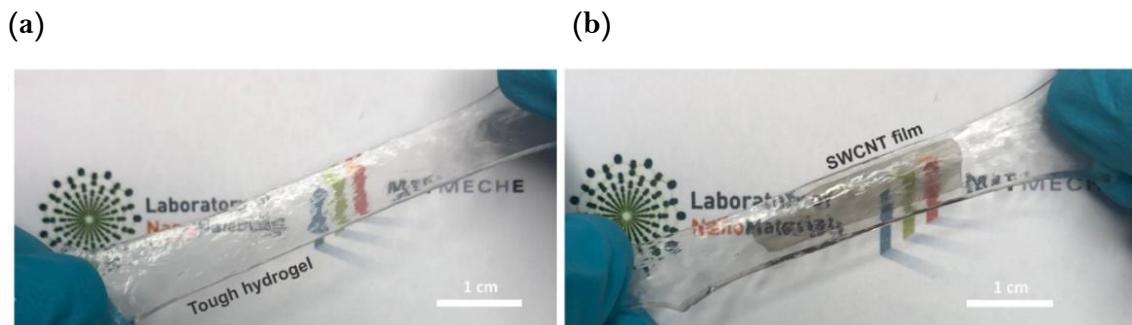
Figure 11. Photographs of tough hydrogel (a) and SWCNT/hydrogel (b) structures at the stretched states demonstrating its high transparency.

3.2.2 Characterization of SWCNT/hydrogel structures obtained on the as-prepared hydrogel

After the SWCNT film deposition by the first approach our structure was ready to be further examined in a special stretching device. For two-point resistance measurements, 2 x 0.5 cm² hydrogel samples with the same size of the SWCNT films are used. Figure 12a demonstrates the electrical properties of the SWCNT films under stretching-releasing cycles with 15, 30, 50% and 100% strains applied. Relative change in the resistance of the SWCNT films between stretched and realeased states are about 40%,

80% and 300% for strains $\varepsilon = 15\%$, 30% and 50%, respectively. When the highest value of strain ($\varepsilon = 100\%$) is applied the resistance reaches 28 kΩ (compared to the initial one of 200 Ω), which can be explained by the appearance of microcracks, visualized by an optical microscope (Figure 12d). After the cracks appear in the SWCNT film, the resistance remains in the range of 16-18 kΩ. However, we demonstrated stable behaviour of fabricated SWCNT/hydrogelstructures, which was observed during 5000 stretching/releasing cycles while 30% strain is applied. Based on the performed characterization it may be proposed that such SWCNT/hydrogelstructures can be used for strain-sensitive applications. Transmittance spectra of the SWCNT/hydrogel structures are presented in Figure 12b. The transmittance value at the wavelength of 550 nm decreases with the increase of the applied strain (Figure 13a). This can be explained by the increase of the scattering in the hydrogel structure while stretching (Figure 14). The scanning electron microscopy (SEM) images of the SWCNT networks after 15%, 30% and 50% strains applied are shown in Figure 12c. SEM studies of the SWCNT/hydrogel structures confirmed slightly changed morphology of SWCNTs after application of these strain values.
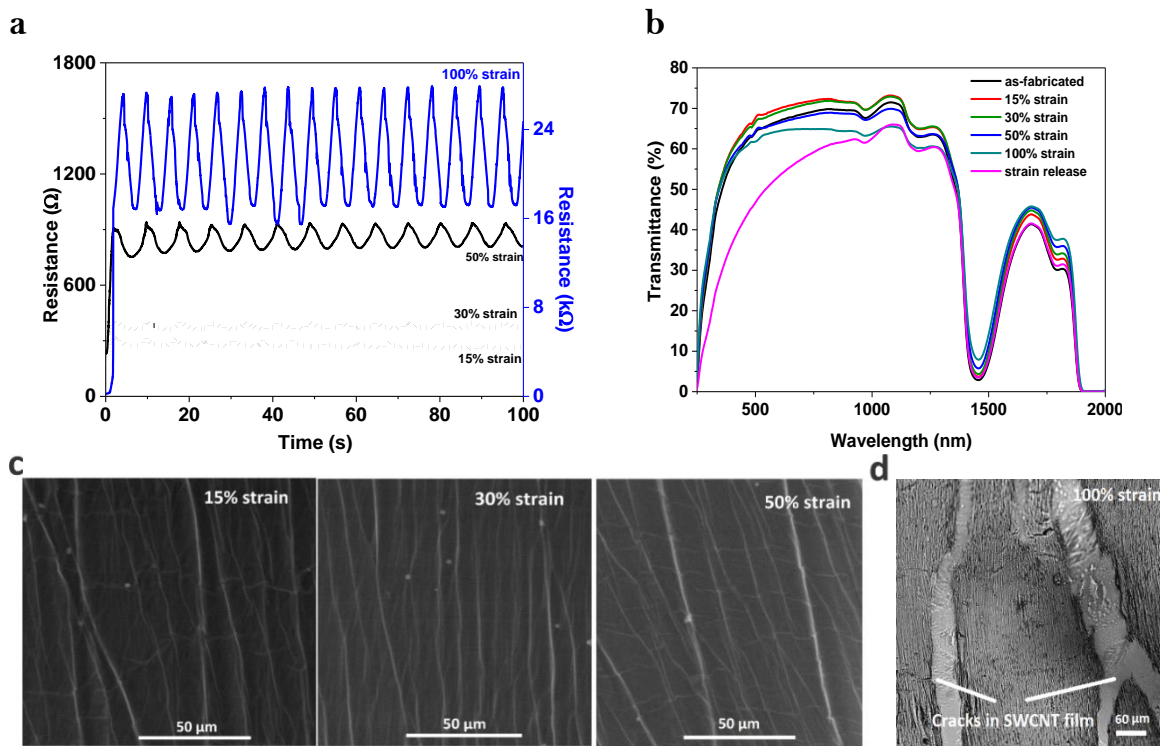
Figure 12. Characterization of SWCNT/hydrogel structures prepared by deposition onto the as-prepared hydrogel: a) resistance change during several stretching/releasing cycles up to 15%, 30%, 50% and 100% strains applied, b) transmittance spectra at different strains, c) SEM images after 15%, 30% and 50% strains applied and d) optical microscopy image of SWCNT film after the 100% strain applied.
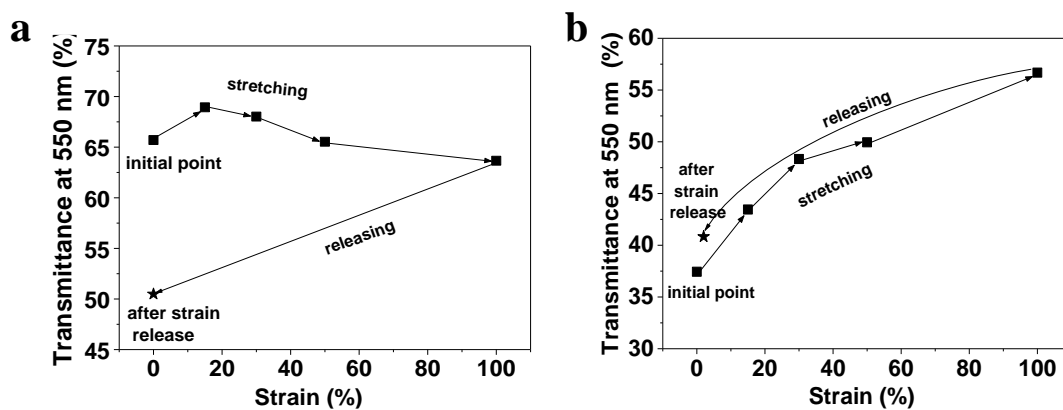
Figure 13. Trend in the transmittance (regular part of full transmittance) change while applying and releasing the strain for the SWCNT/hydrogel structures prepared by a simple dry transferring technique: a) on the as-prepared tough hydrogel; b) on the pre-stretched hydrogel.
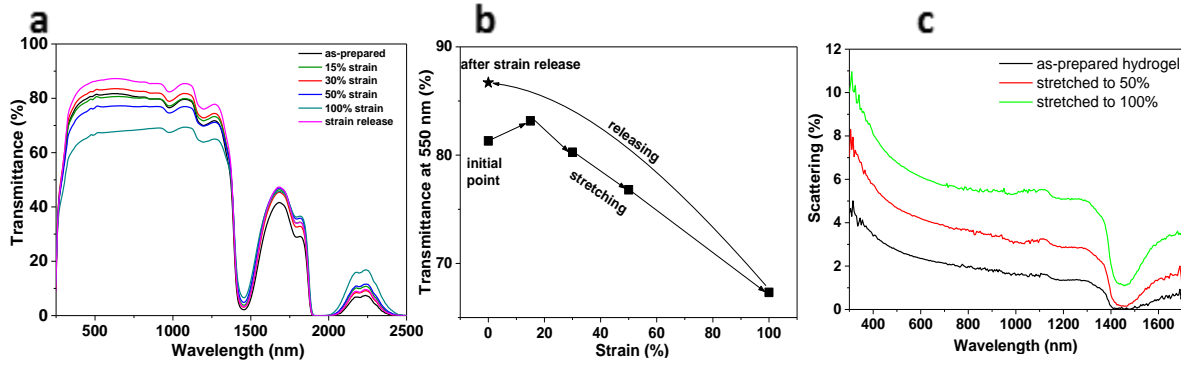
Figure 14. Optical properties of the tough hydrogel: a) transmittance spectra of hydrogel at different stretched states during the first strain and after release; b) trend in the regular transmittance value for the tough hydrogel (at the wavelength of 550 nm); c) scattering spectra (diffusive part of full transmittance) of hydrogel at different stretched states during the first strain and after release.

3.2.3 Characterization of SWCNT/hydrogel structures obtained on the pre-stretched hydrogel

The same characterization is conducted for the second approach with the SWCNT/hydrogel structures on hydrogel pre-stretched to $\varepsilon = 30\%$. It is confirmed that the procedure of the hydrogel substrate pre-stretching before the SWCNT film deposition allows us to exploit formed wrinkles for stable and highly-stretchable electronic components. A relative change in the resistance of the SWCNT film between stretched and released states is about 7% for 15% and 30% strains applied (Figure 15a). When the strain is higher than the pre-stretching strain value, we observe a significant increase of the resistance about 10 times at $\varepsilon = 50\%$ and 60 times at $\varepsilon = 100\%$ applied. However, the resistance value at the 100% strain is still lower for the pre-stretching approach (R = 6 kΩ) than that for the as-prepared hydrogel approach (R = 30 kΩ). The transmittance spectra of the SWCNT/hydrogel structures (Figure 15b) demonstrate an increase in the transparency with the applied strain. This can be explained by the process of wrinkle removal leading to the improvement of the overall transmittance (from the initial value of 37% to 57% while stretched to $\varepsilon = 100\%$). Thus, the pre-stretching approach allows us to improve the transmittance of the whole structure at the stretched state. Moreover, after the strain release, the transmittance returns back to the value of 40% close to the initial

one. Thus, the pre-stretching of the hydrogel before SWCNTs deposition makes possible to overcome the low conductivity at high strains and ensure high transparency. SEM images of the SWCNT/hydrogel structures before pre-stretching and after the strain release are shown in Figure 15c-e. From these images we can observe an excellent adhesion of the SWCNT films to the hydrogel surface before stretching and after the strain release. It is worth noting that the demonstrated approach of the SWCNT/hydrogel composite fabrication can be utilizied for applications, where stable performance of the electrodes during stretching is needed without the alteration of the electrical properties.
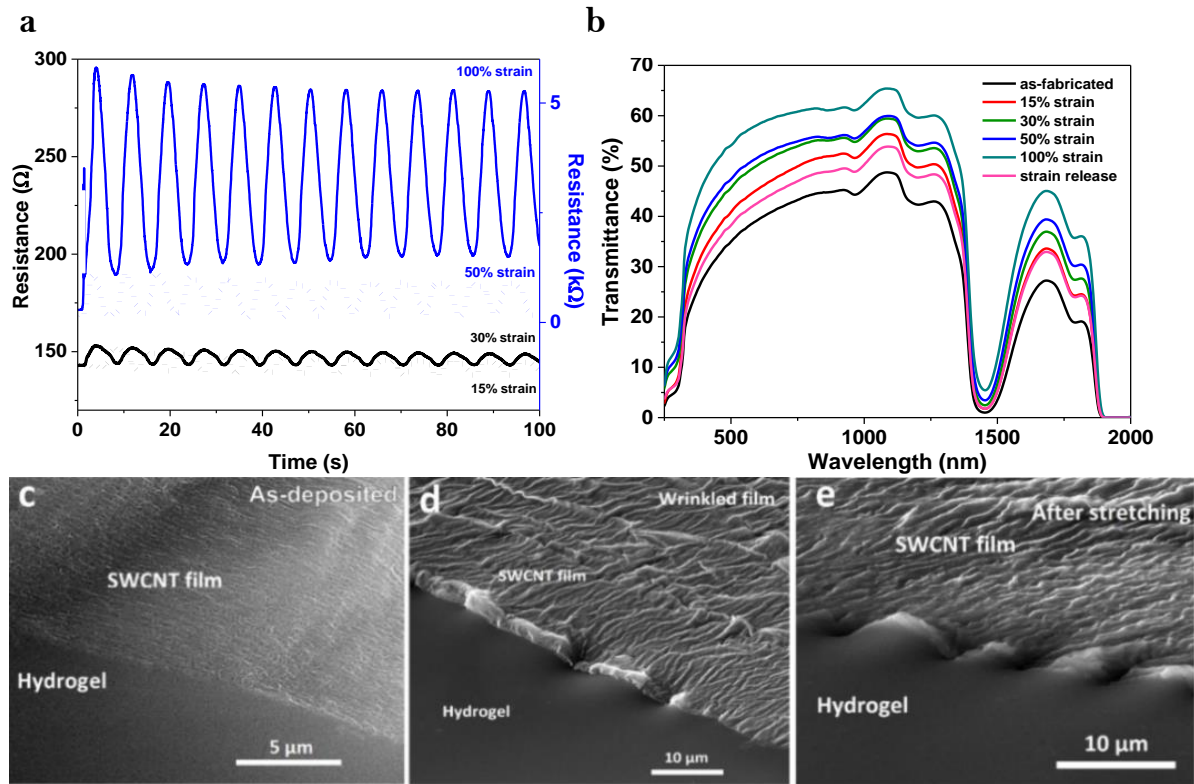
Figure 15. Characterization of SWCNT/hydrogel structures prepared by deposition onto the pre-stretched hydrogel (the pre-strain value is 30%): a) resistance change while 15%, 30%, 50% and 100% strains are applied, b) transmittance spectra at different strains. SEM images of SWCNT/hydrogel structure morphology: c) before release of the hydrogel pre-strain after SWCNT film deposition, d) after release of the hydrogel pre-strain, e) after 15 cycles of stretching to 30% strain.

The resistance (R_l) of the SWCNT/hydrogel structures during stretching is estimated by the Equation 2:

$$R_l = \frac{l}{\sigma_l\, t_l\, w_l},\qquad (2)$$

where σ_l is the electrical conductivity of the SWCNT/hydrogel structures at certain strain; l, w_l and t_l are length, width and thickness of the sample, respectively, at certain strain.

Here we use two assumptions: (i) electrical resistivity of the structure is constant while stretching; (ii) relative change in the SWCNTs and hydrogel dimensions, such as width and thickness, are the same and can be found as [39]:

$$l = l_0(1 + \varepsilon); \qquad w_l = w_0(1 + \varepsilon)^{-\nu}; \qquad t_l = t_0(1 + \varepsilon)^{-\nu}, \qquad (3)$$

where l_0, w_0, t_0 − are lengh, width and thickness of the structure before stretching; ε is applied strain value; ν is the Poisson's ratio ($\nu = 0.4$ for tough hydrogel).

Using Equation 3 and two assumptions, we can express R_l in terms of the stretching:

$$R_l = R_0(1 + \varepsilon)^{1+2\nu}, \qquad (4)$$

where R_0 is the electrical resistance of the SWCNT/hydrogelstructures before stretching.

We use Equation 4 to compare the experimental results and theoretical prediction for the SWCNT/hydrogel resistance change during stretching. The results (Figure 16) reveal a good agreement of the theory with the pre-stretched approach, and thus stable adhession of the SWCNTs to hydrogel, which can be explained by appearance and removal of the SWCNTs wrinkles confirmed by the SEM images. However, disagreement of the theory with the as-fabricated approach is demonstrated due to the structural changes and cracks formation in the SWCNT film while stretching.
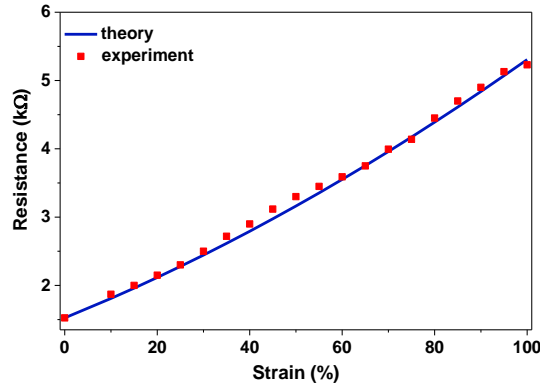
Figure 16. Comparison between experimental results and theoretical prediction for the relative resistance change of the SWCNT/hydrogel structures fabricated by pre-stretched hydrogel approach.

3.2.4 Applications of SWCNT/hydrogel structures

To demonstrate potential applications of our novel material, we develop a stretchable human motion detector based on the SWCNT transfer onto the as-fabricated tough hydrogel and by attaching the SWCNT/hydrogel electrodes (by the hydrogel side) to an arm or to a finger (Figures 17a and b). To avoid mechanical failure at the junction between the stretchable SWCNT/hydrogel structures and rigid wires for signal processing we use an adhesive medical patch, so that the hydrogel directly adhere to the skin. After the fabrication, sensors are attached onto the target places (knuckles and finger flexor). As a result, the skin and SWCNT/hydrogel sensor behave as a single cohesive stretchable object and deformation of the skin can be directly monitored. To detect the relative resistance change from a palm to a fist (relaxed state of the arm (A) and clenched into a fist (B)) we fabricated a SWCNT/hydrogel strain sensor with a 30×5 mm² sensing area (Figure 17a). In order to control small motions, such as particular finger flexing, we fabricate a SWCNT/hydrogel strain sensor with a 10×5 mm² sensing area (Figure 17b). Thus, various types of skin strains could be monitored by the upward and downward trends of the relative resistance data plots. One of the most promising advantages of such devices is the option for repeatable and constant use of the sensor, which does not restrict motions. Moreover, simple encapsulation of the SWCNT films in hydrogel will allow to use such sensors in various implantable devices.
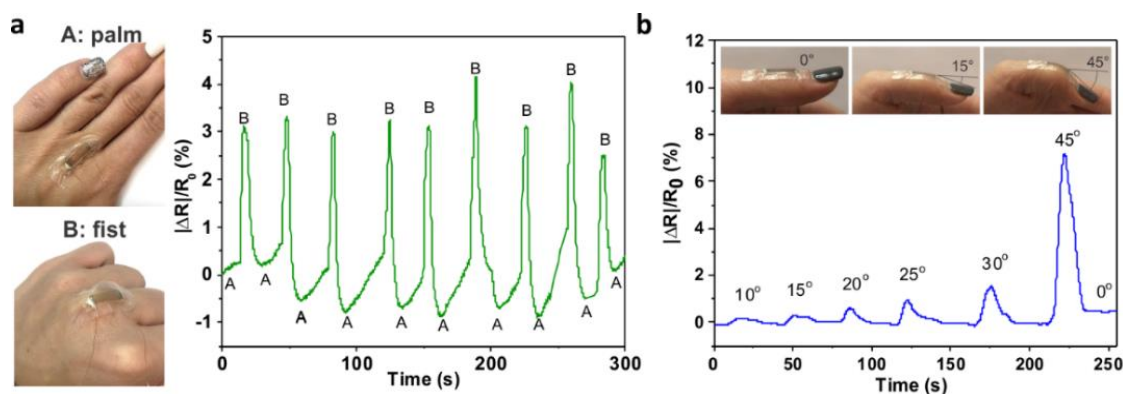
Figure 17. Application of SWCNT/hydrogel structures as active components: a) biocompatible strain-sensors for a human motion detection: resistance change of the SWCNT/hydrogel structure attached to a human arm under repeatable bending cycles, b) resistance change of a SWCNT/hydrogel electrode attached to a human finder depending on the bending angle.

Based on the second pre-stretching approach we fabricated SWCNT/hydrogel based passive electrodes. Figure 18a illustrates a rigid LED-based electronic circuit, which can be mechanically deformed. Previously it has been achieved by a wire connection of LED arrays [40-42], which is rigid and has complicated technology to allow the stretchabilty. Our approach is a novel way of electrical circuit creation, which allows to fabricate biocompatible, transparent, and robust electrodes, stable under large deformations and applicable for different wearable electronic devices. Validation of the performance of the SWCNT/hydrogel structures in an electrical circuit is confirmed by a constant intensity of a LED light under the applied strain. Practically, SWCNT film patterns of any size and shape can be used for different wearable and skin-like devices (Figure 18b). As one more example, we fabricate stable electrode for continuous monitoring of electrocardiography (ECG) signals and its long-term variability, which has improved signal-to-noise ratio (35 dB) compared to commonly used ECG electrodes (30 dB) (Figure 18c). The fact that hydrogels are intrinsically wet will allow them to remain breathable and robust skin contact, revealing its safety for biomedical applications.

39
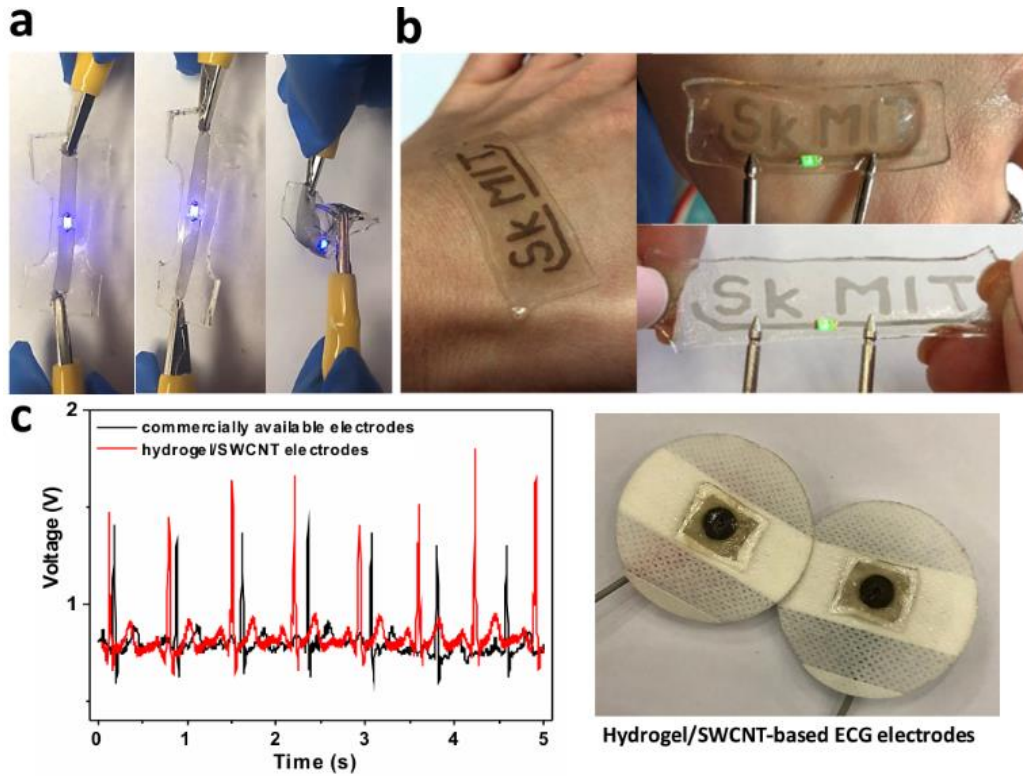
Figure 18. Application of SWCNT/hydrogel structures as passive electrodes: a) stretchable LED-based circuit with conductive SWCNT contacts at different stretched and twisted states, b) SWCNT/hydrogel-based patterned circuits at a relaxed state and stretched to 50 %; c) biocompatible electrodes for ECG signal measurements with photographs of SWCNT/hydrogel electrodes.

However, active and passive element, based on stretchable structures SWCNTs/elastic substrate (demonstrated in Chapters 3.1 and 3.2) required energy storage devices such as supercapacitors, which would be stretchable and transparent as well.

3.3 Stretchable and transparent supercapacitors based on SWCNT films

Transparent energy conversion and storage devices have recently attracted increasing attention due to their great potential as integrated power sources for displays and windows in buildings, automobiles and aerospace vehicles [43-45]. On the other

hand, mechanical stretchability coupled with optical transparency of the energy storage devices is required for many other applications, ranging from self-powered rolled-up displays to self-powered wearable optoelectronics. The design of highly stretchable devices is an essential element in the development of many unprecedented applications such as electronic skin [46, 47] and smart energy storage clothes [48-50]. Portable and wearable supercapacitors, coupled with either self-healability or stretchability [51, 52], have particularly become a mainstream in the personalized electronics [53, 54]. However, the development of both transparent and stretchable supercapacitors (TSSs) is still a challenge, because typical existing electrodes are neither stretchable nor transparent (e.g., metal oxide on carbon-based electrodes), even though they might possess either stretchability with low transmittance (e.g., conducting polymers) or transparency with poor mechanical properties (e.g., ITO and other metal oxides). To our best knowledge, no optoelectronic nor energy-related devices have been reported to show both good transparency and high stretchability, though many devices with only one function have been reported elsewhere e.g. [55-57].

Here, we applied dry deposited thin films of aerosol CVD synthesized SWCNT as the electrodes to fabricate TSSs. Remarkably high specific capacitance and stability are reached with the SWCNT electrodes in test cells and they are used to construct various TSS prototypes. Such devices have attracted much attention from researchers and show promising application potential in the field of wearable energy storage.

3.3.1 TSS based on liquid H_2SO_4/separator

Figure 19 schematically shows the procedure for preparing transparent and stretchable supercapacitors with liquid H_2SO_4/separator. The pristine SWCNTs were first deposited onto a preformed PDMS substrate (Fig. 19a) and then heated to 200°C in order to anneal the surface and to desorb oxygen and organic impurities. After that 2 mol/dm³ H_2SO_4 solution was dropped on top of one of the SWCNT films and covered with a paper separator (Fig. 19b). Finally, we constructed the supercapacitors by assembling another PDMS-supported SWCNT electrode on top of the newly formed separator/liquid H_2SO_4/SWCNT/PDMS multilayer film and glued this structure with

liquid PDMS at the edges. The fabricated supercapacitor is flexible as it can be seen from Fig. 19d and can be stretched at least up to 50% strain, as will be demonstrated further.
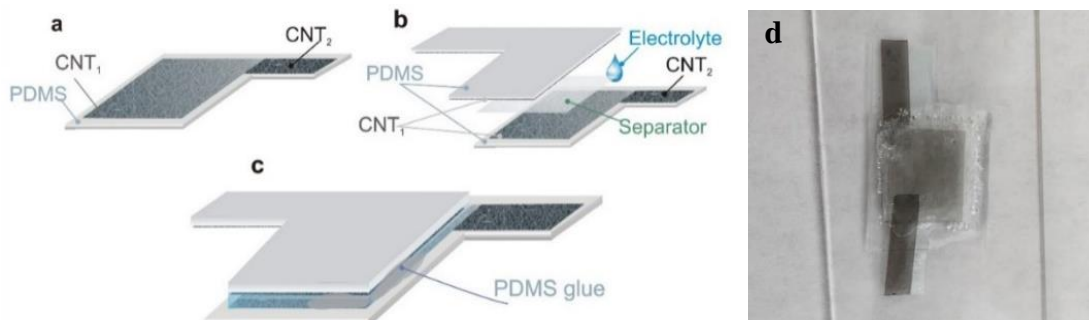
Figure 19. Scheme of TSS fabrication process: (a) deposition of CNT_1 and CNT_2 films on PDMS, (b) Assembling the TSS by adding the separator and acid electrolyte, (c) Gluing two substrates with the liquid PDMS, (d) Photograph of the SWCNT based TSS with H_2SO_4 electrolyte and a nontransparent separator.

Immediately after the liquid PDMS glue was solidified, cyclic voltammogram characteristics were measured at different scan rates from 10 to 500 mV/s (Figure 20). The current increased with the increasing scan rate, as is characteristic for adsorption-controlled reactions, implying that no mass transfer or kinetic limitations can be observed and all the SWCNT surface sites are readily accessible even with the higher scan rates. Thus, the same capacitance is achieved in the studied scan rate range. Due to the fact that we used water based electrolyte and SWCNTs exhibit hydrophobic behavior, cyclic voltammograms measured at different periods of time (Fig. 20a) showed the time dependence. To follow the wetting behavior of the electrodes, the voltammograms were measured immediately after the fabrication process, after 1, 4 and 12 hours. It can be easily seen that after letting the device be impregnated in electrolyte for 12 hours the current increased 6 times.
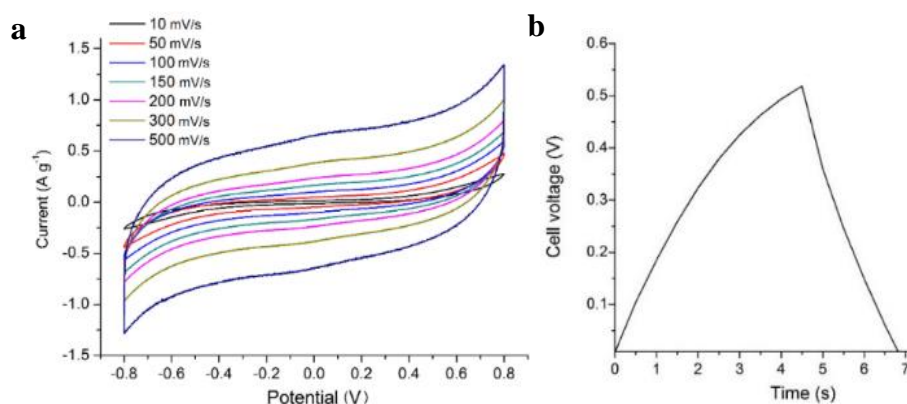
Figure 20. Electrochemical characterization of the SWCNT stretchable supercapacitors with acid H_2SO_4: (**a**) Cyclic voltammograms at various scan rates (numbers indicates scan rates in mV s^{-1}), (**b**) Constant current charging and discharging at 0.25A g^{-1}.

To analyze the stretchability of the transparent supercapacitors, cyclic voltammetric measurements were performed under mechanical deformations, such as stretching after the fabrication process (Fig. 21b). It was observed that the capacitance of the TSS was improved by stretching up to 50% strain. This can be explained by the fact that stretching process led to better wetting of the SWCNTs by the electrolyte, thus increasing the area available for the ion absorption. This type of TSSs has demonstrated the capacitance C_{sp} of 3.2 F g^{-1}, which can be a basis for the comparison with the results obtained for the improved structures.
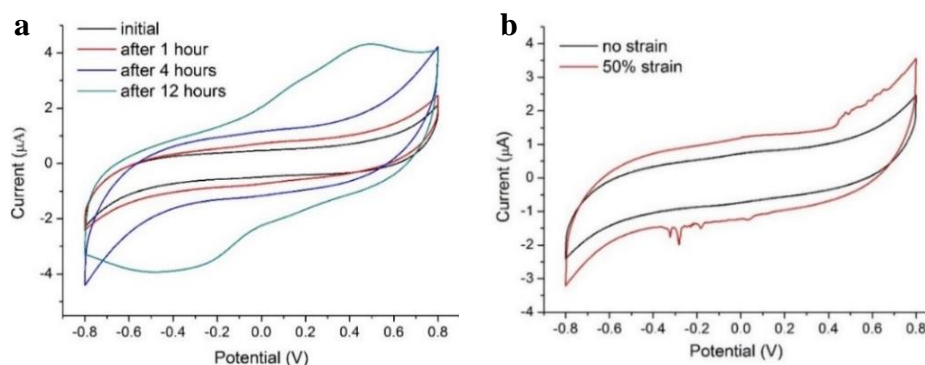
Figure 21. (a) Cyclic voltammorgams of TSS with liquid acidic electrolyte at different periods of time after the fabrication, (b) Cyclic voltammorgams of TSS before stretching and being stretched at 50%.

One of the main issues impeded the fabrication of highly stretchable supercapacitors with high performance is the leakage of the electrolyte while applying force to the supercapacitor. This problem is arisen from the configuration of the stretchable supercapacitor device wherein liquid electrolyte is sandwiched by two electrodes. Our further experiments were devoted to improvement of TSS configuration by replacing the liquid electrolyte, which might suffer from leakage of a harmful liquid, and consequently the non-transparent separator with a conformable gel electrolyte.

3.3.2 TSS based on a PVA-H_2SO_4 gel electrolyte

In order to improve the TSS performance we utilized another type of an electrolyte, polyvinyl alcohol-H_2SO_4 gel. The first two fabrication steps were similar to the ones described in the previously reported section. The last step is deposition of gel viscous solution and pressing one of the electrolyte-coated electrodes on the other electrode. Finally, after the solidification of the gel, the TSS contacting pads were connected to the potentiostat-galvanostat for characterization of the device performance (Figure 22). The whole device can be stretched at least up to 70% strain without any obvious performance change, as it can be seen from Figure 22b. Additional advantages of this supercapacitor is its high transparency – 75% (Figure 22e) and absence of harmful liquid compounds, since the TSS is solid.
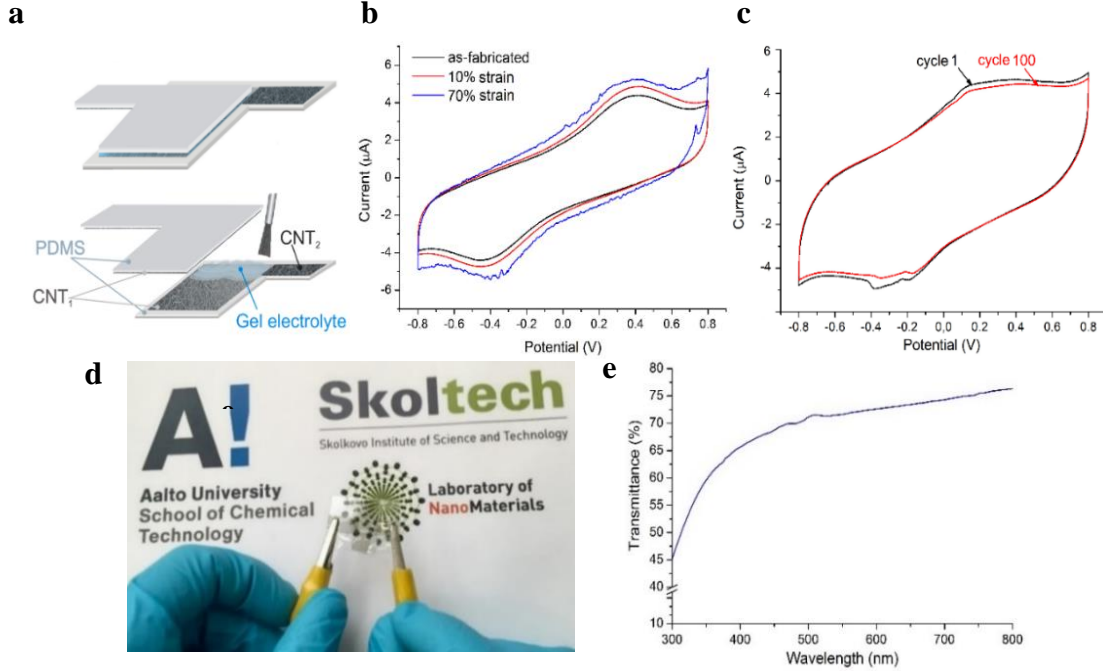
Figure 22. Properties of the TSSs based on gel electrolyte: (a) Schematic image of TSS fabrication process by deposition of gel electrolyte, (b) Electrochemical performance of as-fabricated TSS and under 10% and 70% strains, (c) CV curves for the first and hundredth stretching cycles, (d) Photograph of the TSS, (e) Transmittance spectrum of the device.

The current values can be compared with the values obtained with the acid liquid electrolyte, but the shape of this graph looks better, which indicates better operating parameters of such TSSs. This can be attributed to excellent properties of the PVA-H_2SO_4 electrolyte, less overall resistance because of a thinner electrolyte layer and high tensile strength after solidification, in comparison with TSS based on the liquid electrolyte. The capacitance of the device, C_{sp}, calculated according to Equation 5 achieves the value of 7.4 F g^{-1}:

$$C_{sp} = \frac{1}{2mV\nu} \int_{V_-}^{V_+} I(V)dV. \qquad (5)$$

where m is the mass of the active material in both electrodes, V is the potential window between the positive and negative electrodes, ν - is the scan rate.

Thus, the problems in fabrication of highly stretchable supercapacitors, leakage of the electrolyte, was solved by using the gel electrolyte.

3.3.3 TSS based on a PVA-H₂SO₄ gel electrolyte and pre-stretching approach

For further improvement of TSS characteristics under applied strain we developed pre-stretching approach (Figure 23a), which is based on spreading of gel electrolyte on the SWCNT film under applied strain. We achieved TSS structure, which can be stretched up to 120% of strain without the significant change of the capacitance even after 1000 stretching cycles (Figure 23b). This approach allowed using the effect of better electrolyte diffusion and electron transport through the layers due to pre-straining of the electrodes with deposited gel electrolyte. In Figure 23c, the cyclic voltammograms of the TSS before and after 1000 cycles between -0.8 and 0.8 V are shown and surprisingly, a small improvement in current is seen. This is most likely again due to better electrolyte diffusion over time and indicates excellent stability for the SWCNT electrodes and TSS device.

For this pre-stretching approach, the calculated specific capacitance value of C_{sp} is 17.5 F g⁻¹, which is higher than that obtained for the liquid or gel electrolyte without pre-stretching. It ought to be remarked that recently we have fabricated transparent and flexible electrochemical double-layer capacitor (EDLC) prototype from our SWCNT films. The supercapacitor showed extremely high mass specific capacitance of 178 F g⁻¹ compared to other carbon-based flexible and transparent EDLCs. However, that supercapacitor had higher values of the capacitance due to the fact that material properties were tested in a test cell, and the lateral conductivity of the SWCNT film was not an issue. Therefore, the TSS fabricated here demonstrated relatively high capacitance in a prototype cell being stretchable and transparent.
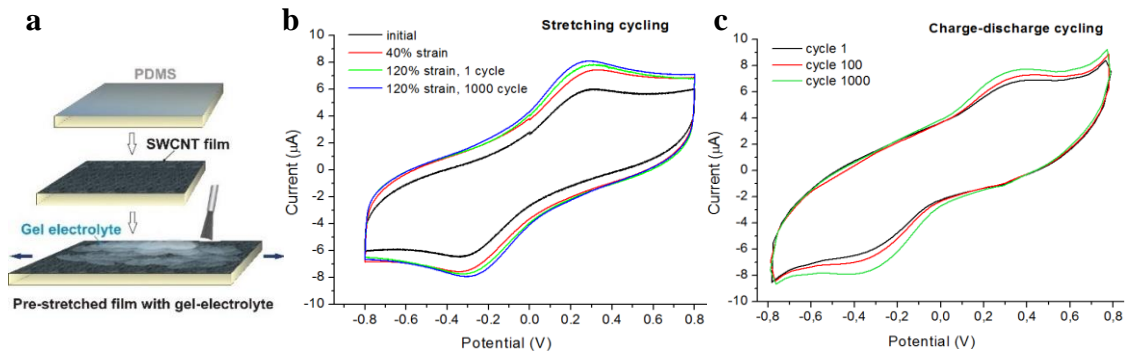
Figure 23. (a) Scheme of gel electrolyte deposition on pre-stretched SWCNTs on PDMS. (b) Cyclic voltammogramms of TSS made of pre-stretched electrodes at zero applied

strain, 40% strain, at first cycle of stretching to 120% and after 1000 cycle of stretching to 120% (scan rate − 200 mV/s), (c) Cyclic voltammogram of the supercapacitor before and after 1000 cycles between -0.8 and 0.8 V.

Thus, we optimized and eventually fabricated highly stretchable TSS by combining our SWCNT films pre-strained on the PDMS substrate and using of a gel electrolyte. The capacitance of these pre-strained TSSs remained nearly unchanged, even under the strain up to 120%. This configuration enabled stretching of the supercapacitor as an integrated unit and overcame the limitation of conventional stretchable supercapacitor configuration wherein two electrodes move relative to the separator under strain. The performance of the stretchable supercapacitors remained nearly unchanged under 120% strain even under stretched conditions and after 1000 stretching cycles. Superior stretchability combined with transparency and high specific capacitance confirmed that fabricated supercapacitor has a great potential for broad practical applications utilizing proposed materials and components. Additionally, such device in a flexible or stretchable form could be further integrated in self-powered consumer electronic system.

3.4 Flexible self-powered piezo-supercapacitor system for wearable electronics

Energy harvesting is essential to achieve independent and sustainable electronic devices, needed in self-powered systems, where no batteries are required, for environmental monitoring and sensing or for biomedical devices in wearable electronic applications [58-61]. Taking forms of irregular air flow/vibration, ultrasonic waves, body movement, and hydraulic pressure, mechanical energy is ubiquitously available in our living environment [62]. For the past decades, energy harvesting from the environment has created a huge impact on the energy sector and thus the scientific community. Therefore, devices, which convert low-frequency vibration and environmental activities (e.g., wind, sound, friction, motion, and thermal energy) into electrical energy through piezoelectric, triboelectric or pyroelectric effects have been implemented [63]. The

harvested energy is sufficient for the operation of small electronic devices in an aperiodic manner using energy storage devices. However, real time generators are required to have effective electrical output and longer cycle stability to support continuous operation in environmental monitoring, defense, and implantable biomedical device applications. Moreover, if such systems are realized in an advanced form, such as flexible, transparent and lightweight, they will immediately become solutions for wearable consumer electronics, serving as both energy harvesters and charging components. Many research groups have attempted to fabricate high performance energy harvesters using different materials and form-factors (e.g., films, fibers, and composites) [59-69].

Piezoelectric materials can convert ubiquitously irregular and low frequency mechanical vibration into electricity and have been extensively studied for the use of energy generators. Piezoelectric fluoropolymers, such as polyvinylidene fluoride (PVDF) and its copolymer poly(vinylidene-trifluoroethylene) (P(VDF-TrFE)), on the other hand, are lightweight, spinnable, soft, and flexible, making them excellent potential candidates for the functional wearable electronics applications [70-72].

Here, we propose to combine and to utilize energy harvesting and storage devices in a flexible manner, with the connection of piezo-harvester and energy storage device as two separate portable and easily dismountable units, without the use of any complicated liquid processes of the system fabrication. Our system consists of solid-state supercapacitor based on single-walled carbon nanotube (SWCNTs) films electrodes and P(VDF-TrFE) metalized film as energy harvester.

3.4.1 Fabrication and characterization of flexible supercapacitor

Figure 24a shows the schematic process flow of the fabrication of the flexible piezo-supercapacitor. Figure 24b shows cross-sectional optical image of the supercapacitor structure, which shows that SWCNTs are fully immersed into the PVA/H_2SO_4 electrolyte, glued between two PET substrates. The whole thickness of the flexible supercapacitor is around 250 μm. Figure 24c is a photograph of the planar flexible supercapacitor in the relaxed state, where the transparency of the device can be observed, and in flexed state (Figure 24d).
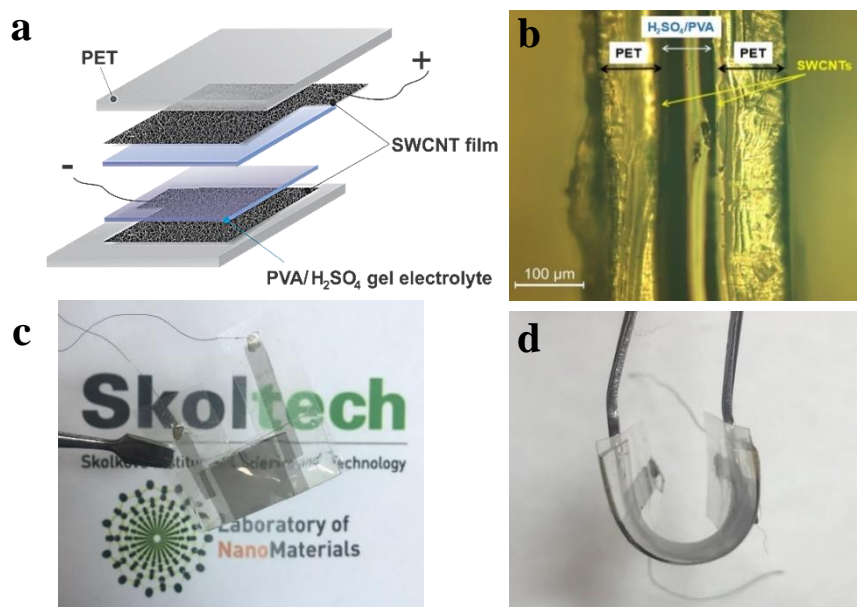
Figure 24. Characterization of the flexible gel-based supercapacitor: (a) Schematic illustration of the flexible supercapacitor fabrication: SWCNT film/PET electrodes are coated with PVA/H_2SO_4 electrolyte and assembled together; (b) cross section of the supercapacitor, which consist of symmetric SWCNT film/PET electrodes and PVA/H_2SO_4 electrolyte. Photographs of the flexible and transparent supercapacitor in relaxed (c) and flexed states (d).

After viscous PVA/H_2SO_4 gel deposited on two SWCNT film/PET electrodes was solidified, CVs characteristics were measured by the potentiostatic procedures at different scan rates from 100 to 1000 mV s^{-1}. Figure 25a shows a typical charging process of the supercapacitor. The current increased with the increasing scan rate, as it is characteristic for adsorption-controlled reactions, implying that no mass transfer or kinetic limitations can be observed and all the SWCNT surface sites are readily accessible even with the higher scan rates. Thus, the same capacitance is achieved in the studied scan rate range. Figure 25b shows the triangle shaped GCD curve of the flexible supercapacitor, which were conducted at 0.25 A g^{-1} (3.25 mA m^{-2}) current value, demonstrating the reversible capacitive behavior.

The specific capacitance of flexible supercapacitor, based on PET/SWCNT electrodes, was calculated to be around 50 F g^{-1}.
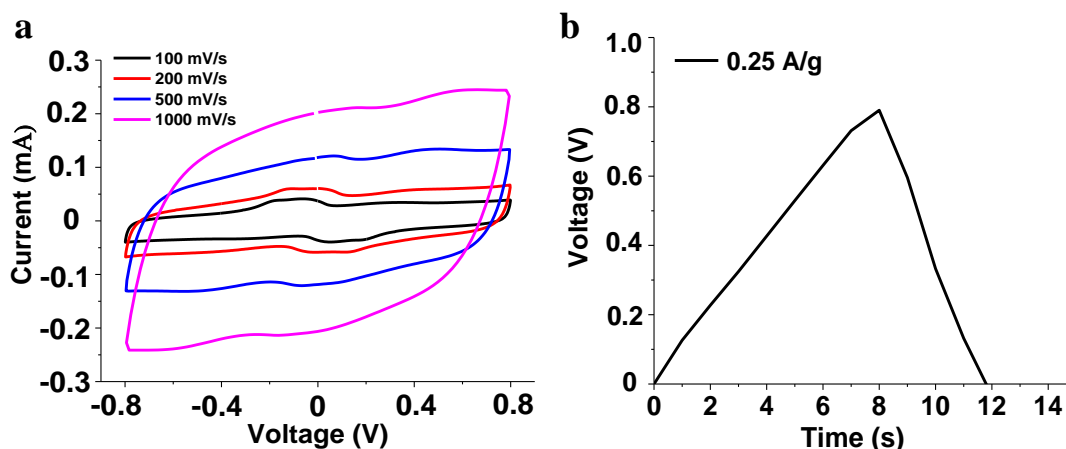
Figure 25. Electrochemical performance of the supercapacitors device with PVA/H$_2$SO$_4$ gel electrolyte: (a) cyclic voltammetry scans of flexible prototype measured at scan rates of 100, 200, 500 and 1000 mV s^{-1}. (b) Galvanostatic charge and discharge curve measured at current of 0.25A g^{-1} (3.25 mA m^{-2}).

3.4.2 Assembly of the piezo-supercapacitor system and measurements of its self-charging performance

The whole piezo-supercapacitor system was assembled in one unit through the rectifying diode-bridge connection. Flexible supercapacitor was fixed on top of the specially designed motorized setup for repeatable mechanical action and connected to the metalized piezo-film, which was fixed inside of the motorized setup frame. Two electrodes of the supercapacitor were connected to the source meter for the measurements of charging processes, occurred during mechanical action of the whole system.

Before charging the flexible supercapacitor, the initial voltage of the device was discharged to zero. After that, the charging process was performed across the piezo-electric P(VDF-TrFE) under external mechanical action by generated voltage potential. The P(VDF-TrFE) film in our system serves as the piezoelectric energy harvester, which can convert mechanical vibration into electricity [73]. This potential, generated by P(VDF-TrFE), can drive the ions in the electrolyte of

the supercapacitor to migrate towards the interface within the symmetric SWCNTs electrodes, establishing a pseudo-capacitance at the interface and storing the electricity in the form of electrochemical energy.

To measure the potential difference obtained on piezo-generator coated with thin metal layers the system was assembled as it is shown in Figure 26a. P(VDF-TrFE) metalized film was used as piezoelectric generator to harvest energy when beat back and forth by a "motorized hand" at a frequency of 2.5 Hz. Figure 26b and c are photographs of the setup with the flexible and transparent supercapacitor connected through the diode-bridge to the P(VDF-TrFE) film, fixed in the frame. Red arrows in Figure 26b, c shows the direction of the "motorized hand" movement: when the deflection angle reaches 30°, frame goes back to the horizontal position while striking the table. Figure 26d shows the output voltage profiles of the P(VDF-TrFE) film with two opposite polarity peaks under a periodic mechanical action. The positive peak corresponds to the stage under compressive force, while the negative peak represents the natural relaxation process. The similar duration of the two stages gives rise to the symmetric characteristics of the amplitude in the two peaks, which dictates the need in charging of the supercapacitor with a rectification unit. Storing the generated energy and driving functional electronic devices require a regulated DC power supply while piezoelectric harvesters generate time-varying voltages; therefore, the rectification is essential. After integration of diode-bridge to the system, the open-circuit voltage generated by the piezo film was measured again. Figure 26f demonstrates repeatable voltage peaks up to 2 V with the same positive polarity, which enables domination of the supercapacitor charging process. For the proper characterization of piezo harvester along with open-circuit voltage short-circuit current is measured. It is observed that piezo-film shows current output close to 300 nA, which is in a good agreement with the previously reported values for such materials (Figure 26e).
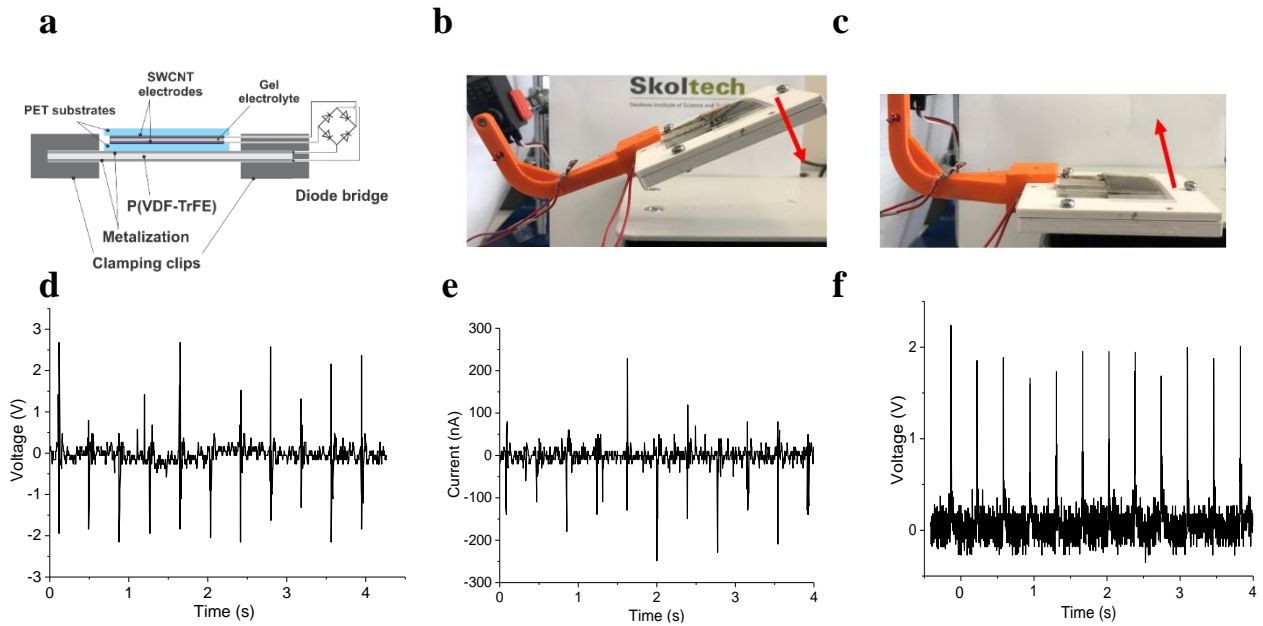
Figure 26. (a) Schematic image of the built piezo-supercapacitor system and (b)-(c) its photographs during the mechanical action testing by a "motorized hand". (d) The open-circuit voltage of as-assembled P(VDF-TrFE) film before rectification and (e) its short-circuit current. (f) The open-circuit voltage of the piezo-film after the diode-bridge integration.

To confirm that the increased voltage of the supercapacitor is a result of the piezoelectric generator, we measured the voltage response of the flexible prototype under the same periodic force conditions. We calculated the average mechanical force applied to the piezoelectric layer during the mechanical action to be about 12.2 N. This value can be commonly obtained by a human hand and considered as a driving force for operation of the device without the use of motorized setup. Figures 27a and b show a typical charging process of the whole device, working as flexible piezo supercapacitor system. According to measured voltage of the flexible supercapacitor, it increased up to 500 mV within 20 s after several repeated beating processes. Based on the obtained values we have calculated the energy density of our system to be 5.06 W h g⁻¹ at a power density - 182.25 W g⁻¹. Moreover, in order to measure the maximum voltage, which can be generated for such type of supercapacitors by piezo-film we measure it during continuous beating process for 100 seconds. As it is shown in Figure 27b the maximum voltage generated by fabricated

piezo-supercapacitor system reached about 650 mV with slight decrease to 600 mV by 100 second.
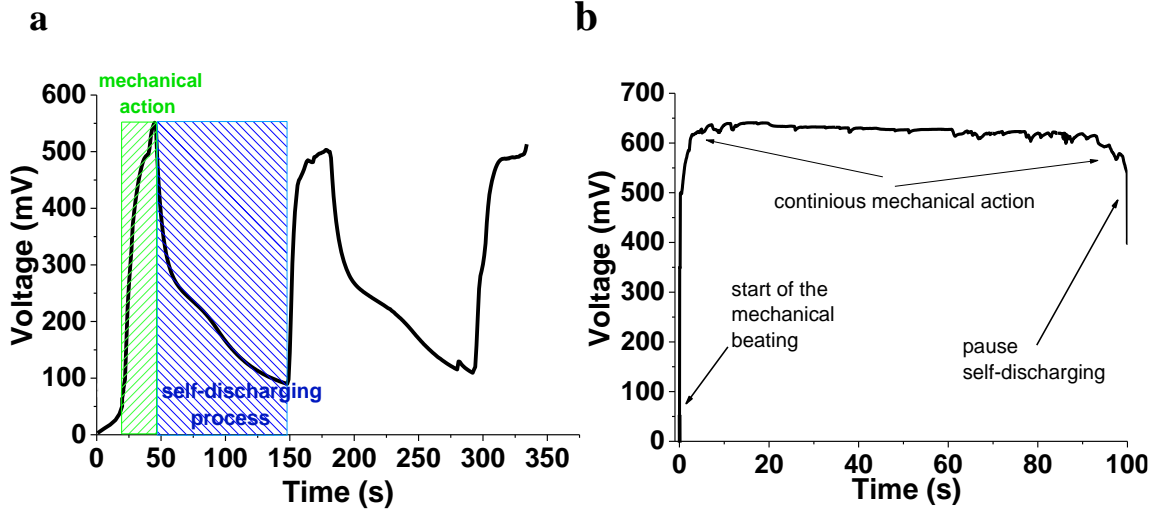
Figure 27. Self-charging performance of piezo-supercapacitor system (a) after several beating cycles and (b) after continuous beating, demonstrating saturated state of the device.

P(VDF-TrFE) is widely investigated due to its excellent mechanical flexibility and high piezoelectric constant. Due to this fact, such material as P(VDF-TrFE) has been already used as a piezo-generator for self-charging power cells. However, voltage response in these works reached up to 300 mV within 240 s [74], 100 mV for 40 s [75], 110 mV for 300 s [76], which is at least six times lower and five times slower than the results, obtained in our work. However, for driving LEDs backlights or powering analog circuits and other small electronic devices it requires low leakage currents and voltages that are higher than the input supply voltage. We propose several strategies to overcome these problems. In order to reduce the leakage current and increase the self-discharging time of the supercapacitor, used in our system, one can reduce the capacitance losses by choice of electrodes and therefore interface of the electrode/electrolyte. As SWCNTs are ideal candidates for flexible device electrodes, they can be modified by various coatings in order to form SWCNTs/oxide and SWCNTs/polymer composite films to enhance the capacitance and stability of the device. Moreover, the increase of the input voltage can be

achieved by integration of tandem device structure, which would consist of sandwiched piezo-films and several supercapacitors connected in parallel; or by the use of step-up DC/DC converter and improved power management design, as it was successfully demonstrated by Niu *et. Al* [77].

Along with the improved design of the whole system, fast discharging and loses in such supercapacitors could be reduced by the improvement of the supercapacitor structure, contribute to lengthen the time of the discharging, which is essential for smooth and longer operation.

3.5 All-nanotube stretchable supercapacitor with low equivalent series resistance

Currently, research in the domain of flexible and stretchable supercapacitors is focused on adjusting electrodes, as they affect the performance the most [78-80]. However, the separator materials for such applications are left relatively unexplored. Besides being dielectric, porous and chemically inert, the separators for stretchable supercapacitors need to withstand multiple bending and stretching without severe structural damages. The materials that meet afore-mentioned requirements are polymers and polymer-based electrolytes, i.e. polyurethane membranes and polyvinyl alcohol (PVA)-based electrolytes [81, 82]. However, despite been inexpensive, non-toxic and highly stretchable, polyurethane membranes made by electrospinning are thicker than any other separator materials (0.2 mm). Other polymer separators (polypropylene, polyethylene), which are normally used in liquid electrolyte systems, offer several advantages, such as good chemical stability, simplicity of manufacturing and processing. However, there are several drawbacks, which are still present and cannot be easily solved. The polymer separators show poor wetting with aqueous electrolytes. Their thicknesses are usually above 20 μm and the attempts to create thinner polymer films usually reveal the problems with their mechanical strength, and as a result they are unable to ensure

reliable short circuit protection. As such separators are not appropriate for stretchable supercapacitor applications, another type of polyvinyl alcohol based electrolytes has been already investigated, which additionally play role of separators and gluing materials and can be stretchable after solidification. The smallest thickness of PVA separator is reported to be 150 μm [83], resulting in relatively high internal resistances. In contrast with separator materials mentioned above, some nanomaterials show outstanding mechanical properties being less than 1 μm thick [84, 85]. In particular, boron nitride nanotubes (BNNTs) is a dielectric nanomaterial that shows high Young's modulus and tensile strength [86]. Generally, the BNNT film is a catalyst-free, dielectric [87, 88], entangled and porous material, chemically inert in strong acids and alkalis [89], composed of incredibly strong individual BNNTs, and thus considered perfect materials for separator applications. So far very few works have been published where the BNNTs utilised as the separator [90, 91]. None of them was either flexible or stretchable. However, due to its remarkable properties, BNNTs are believed to be able to fulfil the requirements of the growing industry and to provide a reliable and stable separator for stretchable supercapacitors.

Here, we applied thin films of SWCNTs as the electrodes and BNNTs as the separator to fabricate all-nanotube stretchable supercapacitors. The SWCNTs and BNNTs films were chosen to be used together due to several important qualities, such as costs, availability and their ideal structures for the use as an electrode and a separator, respectively. The lattice structures, which strengthen the material between walls of both materials, make it possible to test and characterize the device under mechanical stretching. We successfully solved the problem of separator thickness and resistance keeping elastic properties of the device.

3.5.1 Two-electrode cell and electrochemical measurements

We characterized the electrochemical properties of the materials using test cell (Hohsen Corp.) in two-electrode configuration. Figure 28 schematically shows the assembly procedure of the two-electrode test cell. The SWCNT films (1x1 cm²) were transferred by a simple dry-press technique to the top and bottom current collectors.

After this, BNNT dispersions were prepared according to procedure previously described. 1 mg of BNNTs were sonicated in Elmasonic S30 (H) ultrasonic bath with 5 ml of toluene for 15-30 minutes yielding fine dispersion that in less than a minute precipitated and accumulated in the bottom of the vial. A few minutes later, 3 ml of toluene from the upper part of the vial were substituted by 3 ml of DMF with the use of micropipette. The resulting mixture was bath-sonicated for 1-2 minutes. Interestingly, the attempts to disperse BNNTs directly with the DMF/toluene mixture were not successful and produced unstable dispersion. The BNNT separator was deposited onto both SWCNT film electrodes so that it covered the electrode entirely by using airbrush to spread the 5 ml BNNT/toluene-DMF dispersion at 207 kPa with simultaneous heating of the current collectors at 80 °C. Then all the parts were thermally treated at 220 °C for 40 minutes. The thermal treatment is a crucial step as it removes the hydrocarbon residues from the SWCNT synthesis as well as toluene and DMF from the BNNT separator, and thus increases the electrochemical stability of the device. Subsequently, few drops (less than 0.5 ml) of 1M H_2SO_4 liquid electrolyte were added on top of the BNNT separator, and both the top and bottom parts are screwed together (Figure 28).

During the CV measurements, the as prepared cells were cycled at 200 mV s^{-1} for 50 times to stabilize the cell before the data was collected. Subsequently, the CV curves were recorded from 200 to 1000 mV s^{-1} scan rates with 100 cycles for each scan rate. For the scan rate of 200 mV s^{-1} the test cell was further tested for durability under 20 000 CV cycles. GCD measurements were performed at different DC currents throughout the entire potential range up to 25 A g^{-1}. The EIS spectra of the two-electrode test cell have been collected in a potentiostatic mode with the 5 mV amplitude in the frequency range from 1 Hz to 500 kHz with 50 points in total.
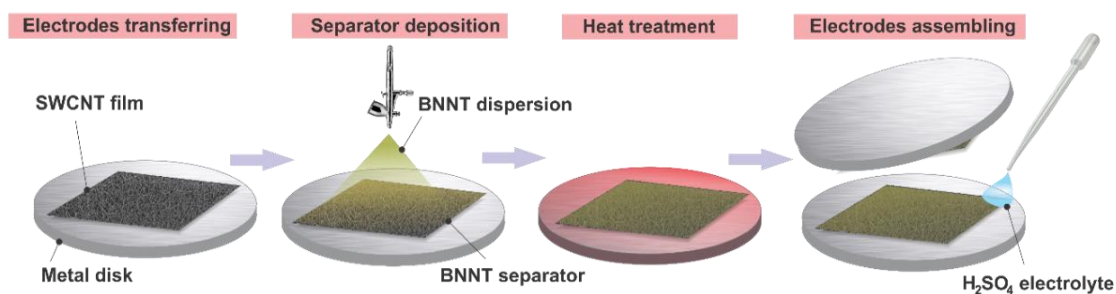
Figure 28. Schematic two-electrode cell assembly process.

3.5.2 Fabrication of the all-nanotube SWCNT/BNNT stretchable supercapacitor prototype

For the stretchable prototype PDMS substrates were prepared. The base and curing agent were mixed with 10:1 ratio by mass, poured onto a laboratory glass, degassed and cured at 90 °C for 40 minutes. After the curing, the sample was cut into rectangular pieces of a desired size. The whole process of SSC assembly is schematically shown in Figure 29. For the SSC prototype fabrication dimethylformamide (DMF) and toluene were replaced by isopropanol (IPA) to prepare the dispersion of BNNTs. This can be explained by the fact that the prototype cannot be heated to remove DMF and toluene from the SWCNT electrode surface and toluene causes swelling of the PDMS substrate. Similarly, BNNTs were sonicated in toluene. After the sonication, 3 cycles of centrifugation in Sigma 3-30KS centrifuge at 6000 RPM for 5 minutes were performed with the subsequent toluene supernatant removal after each step. This was followed by 3 cycles of washing the BNNTs with the equal volume of IPA and centrifugation under the same parameters. The final BNNT/IPA mixture was bath sonicated for 30 minutes yielding a fine dispersion.

After BNNT/IPA dispersion was prepared two electrodes were assembled as follows. The SWCNT film (2x1 cm²) was deposited on top of the first PDMS substrate and 0.5 ml BNNT separator drop-casted from the BNNT/IPA dispersion. The whole structure was heated up to 220°C for 40 minutes. The second PDMS substrate was

57

covered with a thin layer of a PVA/H$_2$SO$_4$ gel-electrolyte and SWCNT films were transferred on top of it. The need for PVA in the supercapacitor prototype is dictated by the fact, that under stretching conditions practically any liquid leaks from the device. To solve this problem, we utilized the solid-state electrolyte (PVA and H$_2$SO$_4$), proven to withstand the mechanical stresses without the electrolyte leakage. It should be noted that the PVA/H$_2$SO$_4$ gel rapidly decomposes when heated, and thus the thermal treatment of the SWCNT films needs to be completed beforehand. After the solvent evaporation, two semi-plates were attached facing each other and glued at the edges with PDMS and left to dry overnight. Here, H$_2$SO$_4$ plays the role of the electrolyte and impregnates the SWCNT electrodes, and the BNNTs act as a separator. Similar techniques, described above for the two-electrode cell, were used for investigation of the electrochemical performance of the fabricated stretchable supercapacitor (CV, GCD and EIS methods).
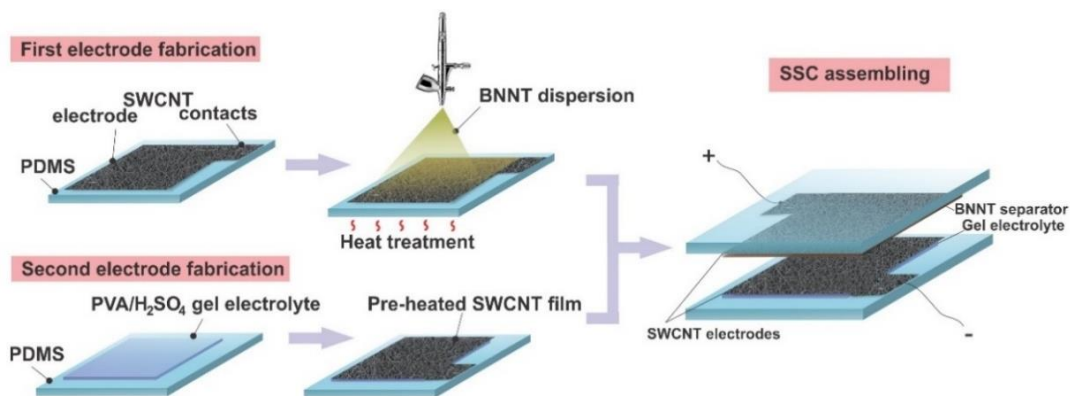
Figure 29. Process flow of stretchable supercapacitor fabrication.

3.5.3 Characterization of all-nanotube SWCNT/BNNT stretchable supercapacitor

The morphology of the BNNT separator on top of the SWCNT film was characterized by SEM (Figure 30a). The BNNT layer forms a porous structure that is beneficial to the SSC in terms of mass transport and ion permeability. In order to estimate the thickness of the separator layer, BNNTs were deposited on the surface of the SWCNT film transferred on an aluminum foil and the cross-section of the structure was cut by

means of SEM FIB. As can be seen from Figure 30b the thickness of the BNNT films utilized for SSC fabrication was around 550 nm.
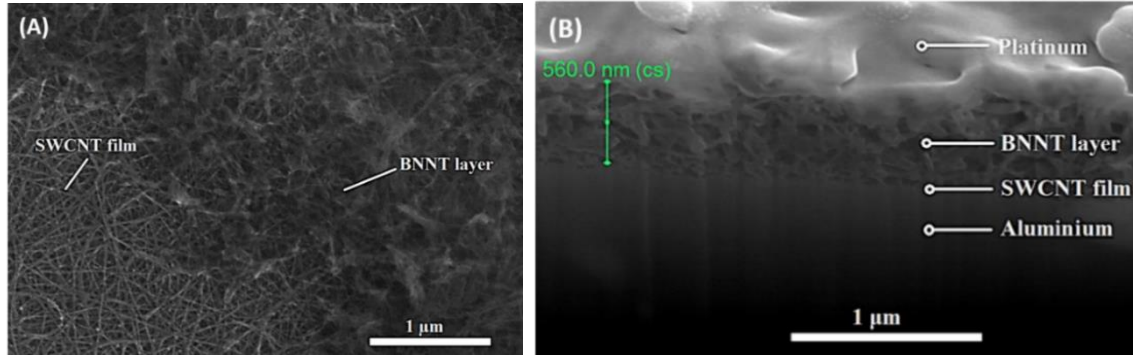
Figure 30. SEM images of the separator layer. (A) BNNT separator on top of the SWCNT film electrode on PDMS, (B) cross-section of the BNNT layer.

Almost rectangular shape of the CV curves (Figure 31a) indicates EDLC capacitance of the cell being measured at 200, 400, 600, 800 and 1000 mV s^{-1} scan rates. Perfect shape of the CVs can be attributed to good transport properties of the BNNT separator. The calculated total capacitance of $C = 105$ μF and specific capacitance of the cell was $C_{sp} = 82$ F g^{-1} or 94 μF cm^{-2}. Here, the areal capacitance (C_A) was calculated using SWCNT electrode mass (m) and area (A) of 1.5 x 1.5 cm^2 – Equations (6) and (7):

$$C = \frac{C_{sp}m}{4}, \tag{6}$$

$$C_A = \frac{2C}{A}. \tag{7}$$

The GCD curves, shown in Figure 31b, demonstrate symmetrical behavior and reflect good performance at different DC currents up to 25 A/g throughout the entire potential range. Additionally, the two-electrode setup was tested for durability under 20000 CV cycles. The specific capacitance retained 96% of its initial value. In order to compare performance of the used materials a two-electrode cell supercapacitor with the commercial separator (25 μm thick Celgard separator purchased from MTI Corporation) was evaluated. As shown in Figure 31d, the Nyquist plots display at the high-frequency

region semi-circles of a similar size for both separators and these are attributed to charge transfer processes on the electrode surfaces. Moreover, the straight lines observed in the low-frequency region represent ion diffusion in the system and the more vertical line suggest improved ion transfer trough the BNNT. The extracted equivalent series resistance (ESR) of the supercapacitor assembled in a test cell with BNNT separator (ESR = 4.6 Ω) is comparable to cell assembled with the commercial one (ESR value of 5.9 Ω).
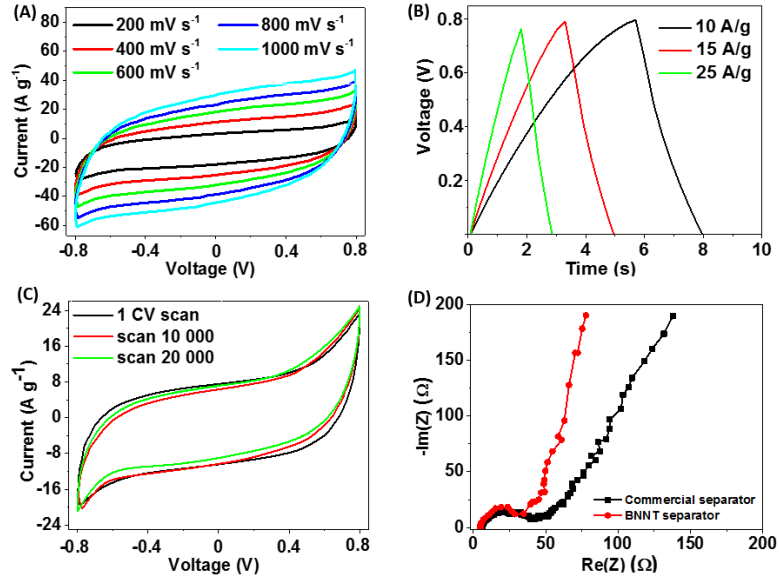
Figure 31. Electrochemical performance of the two–electrode test cell. (A) CV curves at various scan rates. (B) Galvanostatic charge-discharge at high currents. (C) CV curves of 20 000 load cycles collected at a scan rate of 200 mV s⁻¹. (D) Electrochemical impedance spectra of the BNNT separator (blue) and commercial separator (black).

After the material examination, we characterized the stretchable supercapacitor (SSC) prototype in a two-electrode configuration. Figure 32a demonstrates cyclic voltammograms of the fabricated SSC prototype according to the scheme presented previously, at different scan rates. It is worth noting that for the stretchable prototype lower currents and higher impedance obtained in comparison with the test cell. The supercapacitor was stretched up to 25% and 50% strain values for 1000 cycles. CVs at different scan rates and EIS spectra in different stretched positions were measured and shown in Figure 32c and b, respectively. The fabricated SSC could withstand only one stretching cycle with a 55% strain applied due to the limitation in the PDMS substrate

mechanical properties. For the as-fabricated stretchable prototype specific capacitance reached (C_{sp}) 7.7 F g^{-1} and total device capacitance of $C = 20$ µF. Increasing the strain to 50% we observed an increase in the current (Figure 32c). The value of specific capacitance also increase up to 8.4 F g^{-1} due to better electrolyte diffusion while stretching. As it is shown in Figure 32b, the lowest ESR value of 125 Ω was measured by means of EIS after 1000 cycles at 25% strain, which slightly increased to 200 Ω after the 50% strain. This value is still lower than ESR = 250 Ω of the as-fabricated device. It is also noteworthy that the changes in the low-frequency region line in the impedance spectra suggest improved ion transfer with the stretching. Another important finding is that the ESR value of the all-nanotube SSC prototype was two orders of magnitude lower compared to the stretchable supercapacitors with PVA/H$_2$SO$_4$ separator of the similar stretchable configuration (ESR = 15 kΩ). Such a high difference in the ESR yields in a hundred times higher power density of the SSC with the BNNT separator. Additionally, the ESR and capacitance values obtained for the SSC is lower than that of two-electrode test cell supercapacitor, as the test cell electrodes are made of stainless steel, which affects the charge transfer across thr electrodes. It is worth mentioning that for a stretchable supercapacitor the value of the total device thickness (h) was around 1100 µm, including the PDMS substrates, and less than 100 µm excluding it, with the electrode area of the device is 2 x 1 cm². Volumetric capacitance C$_{Vol}$ of the device was calculated according to the eqn (8):

$$C_{Vol} = \frac{C}{A \cdot h}. \tag{8}$$
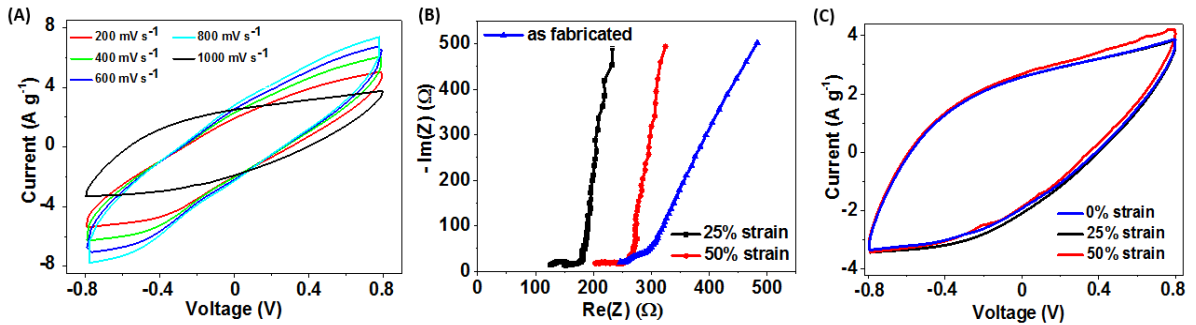
Figure 32. Stretchable supercapacitor characteristics. (A) CVs at different scan rates, (B) EIS spectra of the as-fabricated supercapacitor (blue) after 100 stretching cycles under 25% (black) strain with inset showing ESR of PVA/H2SO4 used for stretchable

supercapacitor, 50% (red) elongation; (C) CVs of as-fabricated SSC device (blue), 25% (black) and 50% (red) strain after 1000 stretching cycles.

According to this formula the as-fabricated SSC exhibits the volumetric capacitance of 0.4 mF cm⁻³. As it was mentioned, the SSC device was stretched up to 50% strain without any significant change in the electrochemical performance. It can be seen from Figure 32c, increasing the strain results in a small increase in the current and consequently in the volumetric capacitance from 0.4 to 0.5 mF cm⁻³.

However, our SSC could withstand only one stretching cycle at 55%, which was explained by appearance of micro cracks in the BNNT separator layer and leading to the short circuit between the SWCNT electrodes. The size of cracks in the BNNT layer was over 10 μm, which is critical for the device performance. Increase in values of volumetric capacitance can be explained by the effect of better electrolyte diffusion and electron transport through the layers due to stretching of the electrodes with the deposited gel electrolyte, which was also discussed in our previous work. Table 3 summarises all calculated values of the as-fabricated SSC device at 0% strain applied and after maximum strain of 50% applied for 1000 stretching/releasing cycles. In order to provide full characterization of the SSC, volumetric energy densities in both stretched and as fabricated conditions were calculated using eqn (9):

$$W = \frac{0.5 \, C_{sp} \, m \, (\Delta V)^2}{4 \cdot 3600 \cdot Vol}, \qquad (9)$$

where *Vol* is the total volume of the device, including both electrodes, separator and substrates volumes. Values of the volumetric capacitance and volumetric energy density for supercapacitors assembled in the test cell were calculated and compared with respective values recalculated for the SSC prototype (excluding the thickness of the PDMS substrate) and are also presented in Table 2. As can be seen, the values of volumetric capacitance for supercapacitors assembled in the two-electrode cell configuration with the commercial separator and with BNNTs separator were calculated to be 7.9 and 8.5 mF cm⁻³, respectively. For the SSC prototype at the initially relaxed state

this value reaches 0.9 mF cm^{-3} while after 1000 cycles of stretching to 50% strain and almost no degradation was observed with slightly increased value of 1.0 mF cm^{-3}.

Table 2. Parameters, calculated for all-nanotube supercapacitors: two-electrode cell assembly and stretchable prototype.

Type of the device assembly	Specific capacitance, C_{sp} (F g^{-1})	Areal capacitance, C_A (μF cm^{-2})	Volumetric capacitance, C_{Vol} (mF cm^{-3})	Volumetric energy density, W (mW h cm^{-3})	Volumetric power density, P (mW cm^{-3})	Equivalent series resistance, ESR (Ω)
Two-electrode cell						
Commercial separator	76	68	7.9	3.5	4800	5.9
BNNT separator	82	73	8.5	3.7	6200	4.6
Stretchable prototype with BNNT separator						
As fabricated	7.7	19	0.9	0.09	32	250
After 1000 cycles of 50% strain	8.4	21	1.0	0.10	40	200

In addition to the volumetric energy density, power density P (W cm^{-3}) of the supercapacitor is also important for the practical applications and could be calculated according to the following Equation 10:

$$P = \frac{\Delta V^2}{4\ ESR \cdot Vol}. \tag{10}$$

The energy density of 3.7 mW h cm^{-3} at the power density of 6200 mW cm^{-3} were obtained for the two-electrodes cell with the BNNTs separator, which is higher than the energy density of 3.5 mW h cm^{-3} at the power density 4800 mW cm^{-3} for the test cell with the commercial separator. The difference can be attributed to slightly lower ESR and smaller thickness of the BNNTs separator. The volumetric energy density for the fabricated and stretched to 50% strain prototype where 0.09 and 0.10 mWh cm^{-3}, respectively, with improved values of volumetric power density from 32 mW cm^{-3} to 40 mW cm^{-3} after the stretching. Such impressive difference in the volumetric energy and power densities values can be explained by lower values of specific capacitances of SSC

and smaller operating voltage window. For further increase of energy density values, the voltage range of the SWCNT electrodes in an aqueous electrolyte can be increased by purifying the SWCNTs form Fe catalyst particles. On the other hand, alternative electrolytes, such as organic solvents or ionic liquids with larger electrochemical window, can be used to increase the energy density values. However, the values of volumetric power densities obtained in this work can be compared with the reported in the literature [92-94] for flexible and stretchable all-solid-state energy storage devices based on similar classes of nanomaterials.

Conclusions

Recent developments in polymer science, thin-film processing, and nanotechnology have demonstrated ultrathin and soft electronic devices which replicates mechanical properties of the skin or can form intimate and robust contact with the skin on polymeric supporting layers. So far, research has generated significant progress in device capabilities, materials exploration, skin-integration techniques, powering systems, and mechanical design, which have produced stretchable and flexible devices capable of providing relevant information in a number of applications. Thus, it is extremely essential to develop and integrate new materials, solutions and methods for novel immerging class of stretchable and transparent electronics.

First of all, we report new transparent, stretchable, conductive and biocompatible structures of elastic polymers (such as PDMS and hydrogels) modified by SWCNT films to create passive electrodes and active sensors for wearable and skin-like electronics. We introduce here a one-step, universal and applicable method for SWCNT/hydrogel and SWCNT/PDMS structures fabrication, withstanding intrinsic stretching up to 100% strain. Our method holds advantages, compared to those reported previously, as it is a direct transfer from the filter onto a hydrogel surface without the need for a sacrificial layer or any other intermediate steps. We apply our approach to create a new set of soft and robust components, such as electrodes for ECG monitoring and active sensors for a human motion detection.

In order to create energy storage devices, which could be further integrated with such active sensors we successfully developed highly stretchable supercapacitors, based on SWCNT films as current collectors and electrode material. All-solid TSS based on PVA–H_2SO_4 gel electrolyte showed specific cell capacitance of 7.4 F g^{-1}. In order to increase durability to stretching of such TSS another technique was performed based on pre-stretching of the electrodes with the deposited gel electrolyte. This approach allowed using the effect of better electrolyte diffusion and electron transport through the electrode layers and obtain the capacitance value of 17.5 F g^{-1}, significantly higher than previously reported. Furthermore, TSS based on pre-stretching approach demonstrated

stretchability up to 120% with excellent stability even after stretching for 1000 cycles in addition to electrochemical stability after 1000 charging–discharging cycles.

Performance of such devices was improved by fabrication of high-performance, stable, low equivalent series resistance, all-nanotube stretchable supercapacitor based on SWCNT electrodes and BNNT separator. The fabrication process is very simple, fast and based on dry transfer and airbrush techniques. The fabricated two-electrode test cell with the materials mentioned above demonstrates excellent stability after 20 000 electrochemical charging/discharging cycles, and EDLC behaviour and retains 96% of its initial capacitance of 82 F g^{-1}. Remarkably, the BNNT separator of only 0.5 μm thickness ensures reliable short circuit protection and low ESR of the SSC. These exciting findings demonstrate that SCs fabricated with the method used in this research hold a great promise for use as high-performance stretchable energy storage devices in the future.

Finally, we have successfully demonstrated the technology of flexible piezoelectric-driven self-charging supercapacitor power cell fabrication, which is based on P(VDF-TrFE) metalized piezo-film and and transparent supercapacitor with SWCNT film/PET electrodes and PVA/H$_2$SO$_4$ electrolyte, which can be used to simultaneously harvest and store the mechanical energy to electrochemical energy. A polarized P(VDF-TrFE) metalized film was fixed in a special "motorized hand" and external mechanical impact establishes a piezoelectric potential across this film, while the whole system produces the mechanical action at a frequency of 2.5 Hz. Piezoelectric film serves as a driving force for flexible supercapacitor charging and therefore storing the energy in the form of electrochemical one. The supercapacitors exhibited the self-charging capability under repeatable applied force and can be charged up to 500 mV in 20 s. At the same time, the maximum voltage generated by fabricated piezo-supercapacitor system reached about 650 mV. The fabrication procedure is simple and could be easily scaled-up to large-scale production. The piezo-supercapacitor system provides a new promising direction in the supercapacitor research for the development of next generation self-powered sustainable power sources for wearable and flexible electronic devices.

Bibliography

[1] S. Harada, K. Kanao, Y. Yamamoto, T. Arie, S. Akita and K. Takei, ACS Nano, 2014, 8, 12851-12857.

[2] H.-H. Chou, A. Nguyen, A. Chortos, J. W. F. To, C. Lu, J. Mei, T. Kurosawa, W.-G. Bae, J. B. H. Tok and Z. Bao, Nat. Commun., 2015, 6.

[3] B. Su, S. Gong, Z. Ma, L. W. Yap and W. Cheng, Small, 2015, 11, 1886-1891.

[4] Y. Hattori, L. Falgout, W. Lee, S.-Y. Jung, E. Poon, J. W. Lee, I. Na, A. Geisler, D. Sadhwani, Y. Zhang, Y. Su, X. Wang, Z. Liu, J. Xia, H. Cheng, R. C. Webb, A. P. Bonifas, P. Won, J.-W. Jeong, K.-I. Jang, Y. M. Song, B. Nardone, M. Nodzenski, J. A. Fan, Y. Huang, D. P. West, A. S. Paller, M. Alam, W.-H. Yeo and J. A. Rogers, Adv. Healthcare Mater., 2014, 3, 1597-1607.

[5] W.-H. Yeo, Y.-S. Kim, J. Lee, A. Ameen, L. Shi, M. Li, S. Wang, R. Ma, S. H. Jin, Z. Kang, Y. Huang and J. A. Rogers, Adv. Mater., 2013, 25, 2773-2778.

[6] D.-H. Kim, N. Lu, R. Ma, Y.-S. Kim, R.-H. Kim, S. Wang, J. Wu, S. M. Won, H. Tao, A. Islam, K. J. Yu, T.-i. Kim, R. Chowdhury, M. Ying, L. Xu, M. Li, H.-J. Chung, H. Keum, M. McCormick, P. Liu, Y.-W. Zhang, F. G. Omenetto, Y. Huang, T. Coleman and J. A. Rogers, Science, 2011, 333, 838-843.

[7] C. S. Haines, M. D. Lima, N. Li, G. M. Spinks, J. Foroughi, J. D. W. Madden, S. H. Kim, S. Fang, M. Jung de Andrade, F. Göktepe, Ö. Göktepe, S. M. Mirvakili, S. Naficy, X. Lepró, J. Oh, M. E. Kozlov, S. J. Kim, X. Xu, B. J. Swedlove, G. G. Wallace and R. H. Baughman, Science, 2014, 343, 868-872.

[8] C.-H. Li, C. Wang, C. Keplinger, J.-L. Zuo, L. Jin, Y. Sun, P. Zheng, Y. Cao, F. Lissel, C. Linder, X.-Z. You and Z. Bao, Nat. Chem., 2016, 8, 618-624.

[9] M.-S. Lee, K. Lee, S.-Y. Kim, H. Lee, J. Park, K.-H. Choi, H.-K. Kim, D.-G. Kim, D.-Y. Lee, S. Nam and J.-U. Park, Nano Lett., 2013, 13, 2814-2821.

[10] S. Harada, W. Honda, T. Arie, S. Akita and K. Takei, ACS Nano, 2014, 8, 3921-3927.

[11] B. K. Sharma, B. Jang, J. E. Lee, S.-H. Bae, T. W. Kim, H.-J. Lee, J.-H. Kim and J.-H. Ahn, Adv. Funct. Mater., 2013, 23, 2024-2032.

[12] Kaltenbrunner, M.; Sekitani, T.; Reeder, J.; Yokota, T.; Kuribara, K.; Tokuhara, T.; Drack, M.; Schwodiauer, R.; Graz, I.; Bauer-Gogonea, S.; Bauer, S.; Someya, T. An Ultra-Lightweight Design for Imperceptible Plastic Electronics. Nature 2013, 499, 458−463.

[13] Yuhao Liu, Matt Pharr, and Giovanni Antonio Salvatore, Lab-on-Skin: A Review of Flexible and Stretchable Electronics for Wearable Health Monitoring, ACS Nano 2017, 11, 9614-9635.

[14] K. Park, D.-K. Lee, B.-S. Kim, H. Jeon, N.-E. Lee, D. Whang, H.-J. Lee, Y. J. Kim and J.-H. Ahn, Adv. Funct. Mater., 2010, 20, 3577-3582.

[15] S. H. Chae, W. J. Yu, J. J. Bae, D. L. Duong, D. Perello, H. Y. Jeong, Q. H. Ta, T. H. Ly, Q. A. Vu, M. Yun, X. Duan and Y. H. Lee, Nat. Mater., 2013, 12, 403-409.

[16] T. Q. Trung and N.-E. Lee, Adv. Mater., 2016, DOI: 10.1002/adma.201603167.

[17] N. Lee and T. Q. Tran, J. Mater. Chem. C, 2017, DOI: 10.1039/C6TC05346G.

[18] Anisimov, A.S., Nasibulin, A.G., Jiang, H., Launois, P., Cambedouzou, J., Shandakov, S.D., Kauppinen, E.I. 2010. Mechanistic investigations of single-walled carbon nanotube synthesis by ferrocene vapor decomposition in carbon monoxide. Carbon, 48, 380-388.

[19] Nasibulin, A.G., Moisala, A., Brown, D.P., Jiang, H., & Kauppinen, E.I. 2005. A Novel Aerosol Method for Single Walled Carbon Nanotube Synthesis. Chem. Phys. Lett., 402, 227-232.

[20] Moisala, A., Nasibulin, A.G., Brown, D.P., Jiang, H., Khriachtchev, L., & Kauppinen, E.I. 2006. Single-walled Carbon Nanotube Synthesis Using Ferrocene and Iron Pentacarbonyl in a Laminar Flow Reactor. Chem. Eng. Sci., 61, 4393-4402.

[21] Nasibulin, A.G., Queipo, P., Shandakov, S.D., Brown, D.P., Jiang, H., Pikhitsa, P.V., Tolochko, O.V., & Kauppinen, E.I. 2006. Studies on mechanism of single-walled carbon nanotube formation. J. Nanosci. Nanotech., 6, 1233-1246.

[22] Lee, K. Y.; Mooney, D. J. Hydrogels for Tissue Engineering. *Chemical Reviews.* **2011**, *101*, 1869−1879.

[23] Aregueta-Robles, U. A.; Woolley, A. J.; Poole-Warren, L. A.; Lovell, N. H.; Green, R. A. Organic Electrode Coatings for next-Generation Neural Interfaces. *Front. Neuroeng.* **2014**, *7*.

[24] Imaninezhad, M.; Kuljanishvili, I.; Zustiak, S. P. A Two-Step Method for Transferring Single-Walled Carbon Nanotubes onto a Hydrogel Substrate. *Macromol. Biosci.* **2017**, *17* (3).

[25] Peppas, N. A.; Hilt, J. Z.; Khademhosseini, A.; Langer, R. Hydrogels in Biology and Medicine: From Molecular Principles to Bionanotechnology. *Advanced Materials.* **2006**, *18*, 1345−1360.

[26] Jeong, J. W.; McCall, J. G.; Shin, G.; Zhang, Y.; Al-Hasani, R.; Kim, M.; Li, S.; Sim, J. Y.; Jang, K. I.; Shi, Y.; et al. Wireless Optofluidic Systems for Programmable In Vivo Pharmacology and Optogenetics. *Cell* **2015**, *162* (3), 662−674.

[27] Lin, S.; Yuk, H.; Zhang, T.; Parada, G. A.; Koo, H.; Yu, C.; Zhao, X. Stretchable Hydrogel Electronics and Devices. *Adv. Mater.* **2016**, *28* (22), 4497−4505.

[28] Liu, X.; Yuk, H.; Lin, S.; Parada, G. A.; Tang, T. C.; Tham, E.; de la Fuente-Nunez, C.; Lu, T. K.; Zhao, X. 3D Printing of Living Responsive Materials and Devices. *Adv. Mater.* **2018**, *30* (4).

[29] Yuk, H.; Zhang, T.; Parada, G. A.; Liu, X.; Zhao, X. Skin-Inspired Hydrogel-Elastomer Hybrids with Robust Interfaces and Functional Microstructures. *Nat. Commun.* **2016**, *7*.

[30] Rogers, J. A.; Someya, T.; Huang, Y. Materials and Mechanics for Stretchable Electronics. *Science.* **2010**, 1603−1607.

[31] Morin, S. A.; Shepherd, R. F.; Kwok, S. W.; Stokes, A. A.; Nemiroski, A.; Whitesides, G. M. Camouflage and Display for Soft Machines. *Science.* **2012**, *337* (6096), 828−832.

[32] Pan, L.; Yu, G.; Zhai, D.; Lee, H. R.; Zhao, W.; Liu, N.; Wang, H.; Tee, B. C.-K.; Shi, Y.; Cui, Y.; et al. Hierarchical Nanostructured Conducting Polymer Hydrogel with High Electrochemical Activity. *Proc. Natl. Acad. Sci.* **2012**, *109* (24), 9287−9292.

[33] Yu, C.; Duan, Z.; Yuan, P.; Li, Y.; Su, Y.; Zhang, X.; Pan, Y.; Dai, L. L.; Nuzzo, R. G.; Huang, Y.; et al. Electronically Programmable, Reversible Shape Change in Two- and Three-Dimensional Hydrogel Structures. *Adv. Mater.* **2013**, *25* (11), 1541–1546.

[34] Guiseppi-Elie, A. Electroconductive Hydrogels: Synthesis, Characterization and Biomedical Applications. *Biomaterials.* **2010**, *31*, 2701–2716.

[35] Shi, Z.; Gao, X.; Ullah, M. W.; Li, S.; Wang, Q.; Yang, G. Electroconductive Natural Polymer-Based Hydrogels. *Biomaterials.* **2016**, *111*, 40–54.

[36] Mawad, D.; Lauto, A.; Wallace, G. G. Conductive Polymer Hydrogels. In *Polymeric Hydrogels as Smart Biomaterials*; **2016**, 19–45.

[37] Ahn, Y.; Lee, H.; Lee, D.; Lee, Y. Highly Conductive and Flexible Silver Nanowire-Based Microelectrodes on Biocompatible Hydrogel. *ACS Appl. Mater. Interfaces* **2014**, *6* (21), 18401–18407.

[38] Sandu, G.; Ernould, B.; Rolland, J.; Cheminet, N.; Brassinne, J.; Das, P. R.; Filinchuk, Y.; Cheng, L.; Komsiyska, L.; Dubois, P.; et al. Mechanochemical Synthesis of PEDOT:PSS Hydrogels for Aqueous Formulation of Li-Ion Battery Electrodes. *ACS Appl. Mater. Interfaces* **2017**, *9* (40), 34865–34874.

[39] Lipomi, D. J.; Vosgueritchian, M.; Tee, B. C. K.; Hellstrom, S. L.; Lee, J. A.; Fox, C. H.; Bao, Z. Skin-like Pressure and Strain Sensors Based on Transparent Elastic Films of Carbon Nanotubes. *Nat. Nanotechnol.* **2011**, *6* (12), 788–792.

[40] Feng, C.; Jiang, L. Y. Investigation of Uniaxial Stretching Effects on the Electrical Conductivity of CNT-Polymer Nanocomposites. *J. Phys. D. Appl. Phys.* **2014**, *47* (40).

[41] Yamada, T.; Hayamizu, Y.; Yamamoto, Y.; Yomogida, Y.; Izadi-Najafabadi, A.; Futaba, D. N.; Hata, K. A Stretchable Carbon Nanotube Strain Sensor for Human-Motion Detection. *Nat. Nanotechnol.* **2011**, *6* (5), 296–301.

[42] Yuk, H.; Zhang, T.; Parada, G. A.; Liu, X.; Zhao, X. Skin-Inspired Hydrogel-Elastomer Hybrids with Robust Interfaces and Functional Microstructures. *Nat. Commun.* **2016**, *7*.

[43] J. S. Huang, G. Li and Y. Yang, A semi-transparent plastic solar cell fabricated by a lamination process, Adv. Mater., 2008, 20, 415–419.

[44] C.-C. Chen, et al., Visibly transparent polymer solar cells produced by solution processing, ACS Nano, 2012, 6, 7185–7190.

[45] H. Y. Jung, M. B. Karimi, M. G. Hahm, P. M. Ajayan and Y. J. Jung, Transparent, Flexible supercapacitors from nanoengineered carbon films, Sci. Rep., 2012, 2, 773–777.

[46] K. Takei, T. Takahashi, J. C. Ho, H. Ko, A. G. Gillies, P. W. Leu, R. S. Fearing and A. Javey, Carbon nanotube active-matrix backplanes for conformal electronics and sensors, Nat. Mater., 2010, 9, 821–826.

[47] S. C. B. Mannsfeld, B. C. K. Tee, R. M. Stoltenberg, C. V. H. H. Chen, S. Barman, B. V. O. Muir, A. N. Sokolov, C. Reese and Z. N. Bao, Highly sensitive flexible pressure sensors with microstructured rubber dielectric layers, Nat. Mater., 2010, 9, 859–864.

[48] D.-H. Kim, N. Lu, R. Ma, Y.-S. Kim, R.-H. Kim, S. Wang, J. Wu, S. M. Won, H. Tao, A. Islam, K. J. Yu, T.-i. Kim, R. Chowdhury, M. Ying, L. Xu, M. Li, H.-J. Chung, H. Keum, M. McCormick, P. Liu, Y.-W. Zhang, F. G. Omenetto, Y. Huang, T. Coleman and J. A. Rogers, Epidermal Electronics, Science, 2011, 333, 838–843.

[49] L. Hu, M. Pasta, F. L. Mantia, L. Cui, S. Jeong, H. D. Deshazer, J. W. Choi, S. M. Han and Y. Cui, Aqueous Supercapacitors on Conductive Cotton, Nano Lett., 2010, 10, 708–714.

[50] B. Yue, C. Wang, X. Ding and G. G. Wallace, Polypyrrole coated nylon lycra fabric as stretchable electrode for supercapacitor applications, Electrochim. Acta, 2012, 68, 18–24.

[51] C. Yu, C. Masarapu, J. Rong, B. Wei and H. Jiang, Stretchable Supercapacitors Based on Buckled Single-Walled Carbon-Nanotube Macro films, Adv. Mater., 2009, 21, 4793–4797.

[52] X. Li, T. Gu and B. Wei, Dynamic and galvanic stability of stretchable supercapacitors, Nano Lett., 2012, 12, 6366–6371.

[53] M. Winter and R. J. Brodd, What are batteries, fuel cells, and supercapacitors?, Chem. Rev., 2004, 104, 4245–4270.

[54] J. B. Kim, et al., Wrinkles and deep folds as photonic structures in photovoltaics, Nat. Photonics, 2012, 6, 327–332.

[56] Z. Yu, X. Niu, Z. Liu and Q. Pei, Intrinsically stretchable polymer light-emitting devices using carbon nanotubepolymer composite electrodes, Adv. Mater., 2011, 23, 3989–3994.

[57] H. Lin, L. Li, J. Ren, Z. Cai, L. Qiu, Z. Yang and H. Peng, Conducting polymer composite film incorporated with aligned carbon nanotubes for transparent, flexible and efficient supercapacitor, Sci. Rep., 2012, 3, 1353–1358.

[58] Pan C, Wu H, Wang C, Wang B, Zhang L, Cheng Z, Hu P, Pan W, Zhou Z, Yang X and Zhu J 2008 Nanowire-based high-performance "Micro Fuel Cells": one-nanowire, one fuel cell *Adv. Mater.* **20** 1644–8.

[59]   Yang Y, Zhang H, Chen J, Lee S, Hou T-C and Wang Z L 2013 Simultaneously harvesting mechanical and chemical energies by a hybrid cell for self-powered biosensors and personal electronics *Energy Environ. Sci.* **6** 1744.

[60] Saravanakumar B, Mohan R, Thiyagarajan K and Kim S-J 2013 Fabrication of a ZnO nanogenerator for eco-friendly biomechanical energy harvesting *RSC Adv.* **3** 16646.

[61] Hwang G T, Park H, Lee J H, Oh S, Park K Il, Byun M, Park H, Ahn G, Jeong C K, No K, Kwon H, Lee S G, Joung B and Lee K J 2014 Self-powered cardiac pacemaker enabled by flexible single crystalline PMN-PT piezoelectric energy harvester *Adv. Mater.* **26** 4880–7.

[62] Jana S, Garain S, Sen S and Mandal D 2015 The influence of hydrogen bonding on the dielectric constant and the piezoelectric energy harvesting performance of hydrated metal salt mediated PVDF films *Phys. Chem. Chem. Phys.* **17** 17429–36.

[63] Wang Z L, Zhu G, Yang Y, Wang S and Pan C 2012 Progress in nanogenerators for portable electronics *Mater. Today* **15** 532–43.

[64] Lin Z-H, Yang Y, Wu J M, Liu Y, Zhang F and Wang Z L 2012 BaTiO3 Nanotubes-Based Flexible and Transparent Nanogenerators *J. Phys. Chem. Lett.* **3** 3599–604.

[65] Mandal D, Yoon S and Kim K J 2011 Origin of piezoelectricity in an electrospun poly(vinylidene fluoride-trifluoroethylene) nanofiber web-based nanogenerator and nano-pressure sensor *Macromol. Rapid Commun.* **32** 831–7.

[66] Park K Il, Jeong C K, Ryu J, Hwang G T and Lee K J 2013 Flexible and large-area nanocomposite generators based on lead zirconate titanate particles and carbon nanotubes *Adv. Energy Mater.* **3** 1539–44.

[67] Garain S, Kumar Sinha T, Adhikary P, Henkel K, Sen S, Ram S, Sinha C, Schmeißer D and Mandal D 2015 Self-poled transparent and flexible UV light-emitting cerium complex-PVDF composite: A high-performance nanogenerator *ACS Appl. Mater. Interfaces* **7** 1298–307.

[68] Chen J, Zhu G, Yang W, Jing Q, Bai P, Yang Y, Hou T C and Wang Z L 2013 Harmonic-resonator-based triboelectric nanogenerator as a sustainable power source and a self-powered active vibration sensor *Adv. Mater.* **25** 6094–9.

[69] Huang C Te, Song J, Lee W F, Ding Y, Gao Z, Hao Y, Chen L J and Wang Z L 2010 GaN nanowire arrays for high-output nanogenerators *J. Am. Chem. Soc.* **132** 4766–71.

[70] Bhajantri R F, Ravindrachary V, Harisha A, Crasta V, Nayak S P and Poojary B 2006 Microstructural studies on BaCl2 doped poly(vinyl alcohol) *Polymer (Guildf).* **47** 3591–8.

[71] Ghosh S. K., Alam Md. M. and Mandal D. 2014 The in situ formation of platinum nanoparticles and their catalytic role in electroactive phase formation in poly(vinylidene fluoride): a simple preparation of multifunctional poly(vinylidene fluoride) films doped with platinum nanoparticles *RSC Adv.* **4** 41886–94.

[72] Mao Y, Zhao P, McConohy G, Yang H, Tong Y, Wang X 2014 Sponge-like piezoelectric polymer films for scalable and integratable nanogenerators and self-powered electronic systems *Adv. Energy Mater.* **4.**

[73] Jana S, Garain S, Sen S and Mandal D 2015 The influence of hydrogen bonding on the dielectric constant and the piezoelectric energy harvesting performance of hydrated metal salt mediated PVDF films *Phys. Chem. Chem. Phys.* **17** 17429–36.

[74] Zhang Y, Zhang Y, Xue X, Cui C, He B, Nie Y, Deng P and Lin Wang Z 2014 PVDF-PZT nanocomposite film based self-charging power cell *Nanotechnology* **25.**

[75] Song R, Jin H, Li X, Fei L, Zhao Y, Huang H, Lai-Wa Chan H, Wang Y and Chai Y 2015 A rectification-free piezo-supercapacitor with a polyvinylidene fluoride separator and functionalized carbon cloth electrodes *J. Mater. Chem. A* **3** 14963–70.

[76] Ramadoss A, Saravanakumar B, Lee S W, Kim Y S, Kim S J and Wang Z L 2015 Piezoelectric-Driven Self-Charging Supercapacitor Power Cell *ACS Nano* **9** 4337–45.

[77] Niu S., Wang X., Yi F., Sheng You Zhou and Zhong Lin Wang 2015 A universal self-charging system driven by random biomechanical energy for sustainable operation of mobile electronics *Nat. Comm.* **6** 8975.

[78] Wang, G., Zhang, L. & Zhang, J. A review of electrode materials for electrochemical supercapacitors. *Chem. Soc. Rev.* 41, 797–828 (2012).

[79] Zhang, F. *et al.* A high-performance supercapacitor-battery hybrid energy storage device based on graphene-enhanced electrode materials with ultrahigh energy density. *Energy Environ. Sci.* 6, 1623 (2013).

[80] Zhao, C., Wang, C., Yue, Z., Shu, K. & Wallace, G. G. Intrinsically stretchable supercapacitors composed of polypyrrole electrodes and highly stretchable gel electrolyte. *ACS Appl. Mater. Interfaces* 5, 9008–9014 (2013).

[81] Jeong, H. T. *et al.* Capacitive behavior of latex/single-wall carbon nanotube stretchable electrodes. *Electrochim. Acta* 137, 372–380 (2014).

[82] Li H. *et al.* Flexible all-solid-state supercapacitors based on polyaniline orderly nanotubes array. *Nanoscale*, 9, 193 (2017).

[83] Meng, C. Z., Liu, C. H., Chen, L. Z., Hu, C. H. & Fan, S. S. Highly Flexible and All-Solid-State Paper like Polymer Supercapacitors. *Nano Lett.* 10, 4025–4031 (2010).

[84] Zhang, H. Ultrathin Two-Dimensional Nanomaterials. *ACS Nano* 9, 9451–9469 (2015).

[85] Zhang R., Cheung R., Two-dimensional Materials - Synthesis, Characterization and Potential Applications, ISBN 978-953-51-2555-6 (2016).

[86] Arenal, R., Wang, M.-S., Xu, Z., Loiseau, A. & Golberg, D. Young modulus, mechanical and electrical properties of isolated individual and bundled single-walled boron nitride nanotubes. *Nanotechnology* 22, 265704 (2011).

[87] Kim, K. S. *et al.* Polymer nanocomposites from free-standing, macroscopic boron nitride nanotube assemblies. *RSC Adv.* 5, 41186–41192 (2015).

[88] Huang, C. & Grant, P. S. One-step spray processing of high power all-solid-state supercapacitors. *Sci. Rep.* 3, 2393 (2013).

[89] Chopra, N. G. *et al.* Boron Nitride Nanotubes. *Science*, 269, 966–967 (1995).

[90] Diana Santiago de Jesus D., *NASA Glenn Research Center Technical report* (2012).

[91] Demuth Derek Christian, *Electrical & Computer Engineering Theses & Dissertations*, 6 (2016).

[92] Li N. *et al.* Compact graphene/MoS_2 composite films for highly flexible and stretchable all-solid-state supercapacitors. *J. Mater. Chem. A.* 5, 3267 (2017).

[93] Meng, Y. *et al.* All-graphene core-sheath microfibers for all-solid-state, stretchable fibriform supercapacitors and wearable electronic textiles. *Adv. Mater.* 25, 2326–2331 (2013).

[94] Gu T, Wei B. Fast and stable redox reactions of MnO_2/CNT hybrid electrodes for dynamically stretchable pseudocapacitors. *Nanoscale* 7, 11626–11632 (2015).

[95] Xu Y, Lin Z, Huang X, Wang Y, Huang Y, Duan X., Functionalized graphene hydrogel-based high-performance supercapacitors, Adv Mater. 2013 Oct 25; 25 (40):5779-84.